

Effects of trapped particle dynamics on the structures of a low-frequency shear Alfvén continuous spectrum

Ilija Chavdarovski^{1,2} and Fulvio Zonca¹

¹ Associazione Euratom-ENEA sulla Fusione, C.R. Frascati, C.P. 65 - 00044 Frascati, Italy

² Department of Physics, University of Tor Vergata, Via Della Ricerca Scientifica 1, 00133, Rome, Italy

Received 20 April 2009, in final form 11 August 2009

Published 13 October 2009

Online at stacks.iop.org/PPCF/51/115001

Abstract

We analytically derive the structures of the low-frequency shear Alfvén continuous spectrum due to resonant wave–particle interactions with magnetically trapped thermal particles in tokamaks. Our theoretical description asymptotically recovers known results in the relevant limits at both high and low frequencies; furthermore, it is relevant for assessing the accurate kinetic structures that are due to shear Alfvén and acoustic wave spectra in toroidal geometry. Since there is a continuous transition between various shear Alfvén wave and MHD fluctuation branches in many situations of experimental interest, the results reported in this work are of practical relevance for their interpretation when used in the theoretical framework of the general ‘fishbone-like’ dispersion relation.

1. Introduction

Since the early observation of beta induced Alfvén eigenmodes (BAE) [1, 2], connected with significant redistribution of supra-thermal ions generated by neutral beam ion (NBI) heating [1], significant attention has been devoted to exploring low-frequency Alfvénic fluctuations in toroidal confinement devices. Here, by low frequency we mean $|\omega| \ll \omega_A \equiv v_A/qR_0$, with $v_A = B/\sqrt{4\pi\bar{\rho}}$ the local Alfvén speed, $\bar{\rho}$ the plasma mass density, q the safety factor and R_0 the torus major radius. In this way, a ‘zoology’ of Alfvénic fluctuations was described by experimental observations [3], which can all be put in a single and general theoretical framework [4–12]. Within the ‘Alfvén zoo’ (see [13] for a recent review), ‘low-frequency specimens’, which have attracted significant attention due to their application as diagnostic tools [14, 15], are the Alfvén cascades (ACs) [14] observed in JET (also known as reversed shear Alfvén eigenmodes (RSAEs) [16] from their observation in JT-60U).

A variety of experimental observations have recently renewed the interest in the detailed structures of the Alfvén continuum at low frequencies: observation of a broad band discrete Alfvén spectrum (DIII-D with toroidal mode numbers in the range $n \sim 2\text{--}40$) excited by

both energetic ions (low- n) and thermal ions (high- n) [17]; evidence of ‘low-frequency feature’ of ACs [18] and finite frequency fishbone oscillations at the geodesic acoustic mode (GAM) frequency [19, 20] (JET); BAE excitations by finite amplitude magnetic islands (FTU [21, 22], TEXTOR [23]); observation in NSTX and JET of beta induced Alfvén acoustic eigenmodes (BAAEs) [24, 25] at frequencies below the ‘BAE accumulation point’ ($|\omega| < \omega_{\text{BAE}} \approx q\omega_{\text{T}_i} \equiv v_{\text{T}_i}/R_0$, with ω_{T_i} the thermal ion transit frequency, $v_{\text{T}_i} = (2T_i/m_i)^{1/2}$ the ion thermal speed, T_i the ion temperature and m_i their mass) of the low-frequency shear Alfvén wave (SAW) continuous spectrum [7]; and more recently the evidence of ‘Sierpes modes’ in ASDEX Upgrade (AUG) [26, 27], interpreted as BAE excited by energetic ions generated by ion cyclotron resonance heating (ICRH) [28–30], and of ICRH driven BAE in Tore Supra [31].

In the same frequency range, it is worthwhile recalling the many observations of GAM structures in different devices: DIII-D [32], TEXT [33], CHS [34], JIPPT-IIU [35], T10 [36], JFT-2M [37], AUG [38], HL-2A [39] and TEXTOR [40]. Such structures interact with MHD and SAW fluctuations and play an important role in the long time scale behavior of burning plasmas. In fact, at frequencies of the order of the thermal ion transit frequency, MHD as well as low-frequency SAW fluctuations and drift wave turbulence (DWT) occur on similar time scales, facilitating cross-scale couplings [9, 11, 41–44] that occur mostly due to their mutual interactions via zonal flow (ZF) [45] and GAM [46] generation or corrugation of radial equilibrium profiles [41, 47, 48].

The low-frequency SAW spectrum can be excited by both energetic as well as thermal particles, as predicted theoretically [7, 8, 49, 50] and confirmed by many recent experimental observations [17, 27, 31, 51–57]. Energetic ions can also excite GAM via velocity space anisotropy of their distribution function [58–63]. Meanwhile, there are close relationships between BAE and GAM spectra, which have lately been emphasized and discussed [8–10, 12, 64, 65]. These elements are of considerable interest since they confirm the conceptual framework summarized above for describing mutual interactions of SAW/MHD/DWT on long time scales.

When the energetic ion drive is sufficiently strong, experimental observations clearly indicate that there is a continuous transition between various SAW and MHD fluctuation branches [19, 20, 51, 55, 57], consistent with theoretical predictions [4–6, 66–68]. This transition can be described by one single and general ‘fishbone-like’ dispersion relation in the form [4–11]

$$i\Lambda(\omega) = \delta\hat{W}_f + \delta\hat{W}_k, \quad (1)$$

which is based on the two scale-length essence of singular (inertial/kinetic) and regular (ideal MHD) structures of the underlying fluctuations. Here, the left-hand side (lhs) is the inertial (kinetic) layer contribution due to thermal particles, while the right-hand side (rhs) comes from background MHD and thermal/energetic particle kinetic contributions in the regular ideal regions. Equation (1) neglects finite ion Larmor radius and magnetic drift orbit width effects, which are discussed in [49] and more recently in [12, 22]. Note also that equation (1) was originally derived for modes with dominant flute-like structure ($|k_{\parallel}qR_0| \ll 1$) and for high- n so that ion diamagnetic and transit frequency can be comparable. The inertial layer contribution is readily extended to either consider the degeneracy removal between poloidal sidebands parallel wave-vectors at finite $|k_{\parallel}qR_0|$ [28–30, 69] and/or between poloidal sideband diamagnetic effects at moderate or small poloidal mode number m [20, 29, 30]. With these extensions, equation (1) describes the entire ‘Alfvén zoology’ of SAW, including BAAE [69]³

³ Reference [69] demonstrates that $\Lambda^2 = k_{\parallel}^2 q^2 R_0^2$, which is the general form of the SAW continuum at low frequency [7, 49, 50], is also the ‘general dispersion relation applicable for the Alfvén-acoustic continuum’.

with kinetic singular layer at $k_{\parallel}qR_0 = 0$ and MHD fluctuations [10, 20]. Equation (1) can then be straightforwardly generalized to BAAE and other SAW modes at finite $|k_{\parallel}qR_0|$ [5, 6, 8, 9, 11] following the asymptotic matching procedure used to investigate toroidal Alfvén eigenmodes (TAEs) [70, 71].

Recent experiments on JET [24, 25, 58, 72] and NSTX [24, 25, 55] as well as DIII-D [56, 73] show the existence of modes below the accumulation point frequency of the continuous SAW spectrum at low frequencies (ω_{BAE}). These modes belong to both SAW and GAM spectra, but we consider them here on the same footing since $\omega_{\text{BAE}} = \omega_{\text{GAM}}$ in the long wavelength limit [8–10], and BAE/GAM fluctuations are distinguishable mainly via mode polarization [8–10, 12, 64, 65, 74] and excitation mechanism (isotropic versus anisotropic particle distribution function in velocity space) [7, 12, 49, 50, 58, 59, 75]. Symmetry breaking mechanisms, which remove the BAE/GAM degeneracy at sufficiently short wavelength, are due to finite ion diamagnetic frequency [8–10, 65] as well as finite electron magnetic drift frequencies and finite electron inertia [74]. At $|\omega| < \omega_{\text{BAE}}$, BAAE modes [24, 25] with generally mixed Alfvén-acoustic polarizations [24, 25, 64, 74] are also possible.

As discussed above, various physics become important at frequencies that are typically below ω_{BAE} , such as coupling of SAW with the slow magneto-acoustic wave (SMW) and kinetic effects due to both circulating as well as trapped particles (ions and electrons) in the long mean free path collisionless limit [76]. For modes excited near the ‘BAE accumulation point’ of the low-frequency SAW continuum, taking the fluid limit $|\omega| \gg \omega_{\text{Ti}}$ of kinetic equations is justified for either $T_e \gg T_i$ or $q \gg 1$ [7] since, in these limits, $\omega_{\text{BAE}} \simeq q\omega_{\text{Ti}}(7/4 + T_e/T_i)^{1/2}$ and magnetic drift ion Landau damping is exponentially small. However, direct comparisons of kinetic and fluid limit expressions of the SAW continuum accumulation point, $\Lambda(\omega) = 0$ from equation (1), show that the validity range of fluid expressions is very limited [7, 20]. Similar considerations apply to GAM frequency expressions [65] and follow directly from the argument on BAE/GAM degeneracy [8–10]. Thus, kinetic theories of both BAE [7, 12, 49, 50, 74, 75] and GAM [65, 77–79] are generally needed. Kinetic theory is generally needed also for BAAE [69, 80, 81], since $\omega_{\text{BAAE}} \sim (T_e/T_i)^{1/2}\omega_{\text{Ti}}$ from fluid limit estimates and strong wave-particle resonant interactions are expected.

In general, it is of practical importance to extend theoretical analyses to even lower frequencies, since there is a continuous transition between various SAW and MHD fluctuation branches in many situations of experimental interest [19, 20, 51, 55, 57]. When $|\omega| \lesssim \omega_{\text{Bi}} \equiv (r/R_0)^{1/2}(T_i/m_i)^{1/2}/(qR_0) \approx \epsilon^{1/2}\omega_{\text{Ti}}$, trapped thermal ion dynamics and bounce-averaged trapped thermal electron response become important and need to be taken into account [20, 29, 30]. Here, ω_{Bi} is the bounce frequency of deeply trapped ions between magnetic mirror points, r is the radial flux coordinate ranging from $r = 0$ (magnetic axis) to $r = a$, with a the plasma minor radius, and $\epsilon = r/R_0$ is the tokamak local inverse aspect ratio. In this work, we extend previous investigations [7] and generalize the expression of Λ in equation (1) to $0 < |\omega| < \omega_{\text{BAE}}$ by inclusion of trapped particle dynamics. Because of their small mass, trapped electrons contribute to $\delta\hat{W}_{\mathbf{k}}$ via resonant ($\omega = \bar{\omega}_{\text{de}}$) as well as non-resonant responses only via their bounce averaged dynamic behavior, although kinetic layer physics may be modified at sufficiently short wavelength by finite electron magnetic drift frequencies and finite electron inertia [74]; bounce-averaged trapped ion dynamics contributes to $\delta\hat{W}_{\mathbf{k}}$ as well and its effect may be of crucial importance in determining the internal kink mode stability in ITER because of ion Landau damping due to the precession resonance ($\omega = \bar{\omega}_{\text{di}}$) with thermal ions [82]. Here, $\bar{\omega}_{\text{ds}}$ (for $s = e, i$) are the magnetic drift orbit precession frequencies for electrons and ions; in particular, $\bar{\omega}_{\text{ds}} = \bar{\omega}_{\text{Ds}}m_s v^2/2T_s$ for deeply trapped particles, where $\bar{\omega}_{\text{Ds}} = (nq/r)T_s/m_s R_0 \omega_{\text{cs}}$ and $\omega_{\text{cs}} = e_s B/m_s c$ is the cyclotron frequency of each species. We treat wave-particle resonant interaction and SAW-SMW coupling on the same footing

and show that, for $|\omega| \ll \omega_{\text{Bi}}$, the trapped thermal ion contribution is not only important, but becomes dominant and of order $\epsilon^{-1/2}$ with respect to that of circulating particles. Hence, it is of crucial importance to include trapped thermal ion dynamics for deriving the correct local dispersion relation for SAW/SMW spectra in toroidal geometry [20, 29, 30].

In this paper, we show that our extended Λ expression asymptotically recovers known results: at low frequency, $|\omega| \ll \omega_{\text{Bi}}$, the Graves and Hastie [83] form of the MHD inertia enhancement [84–88] is reproduced, whereas at high frequencies, $\omega_{\text{Bi}} \ll \omega_{\text{Ti}} \approx |\omega| \ll \omega_{\text{A}}$, the former kinetic theory result of [7] is obtained. As corollaries of our derivation, we confirm prior results showing BAE/GAM degeneracy in the long wavelength limit [8–10] and the identity [10, 65] of the MHD inertia enhancement factor to the ZF polarizability induced by ion temperature gradient (ITG) turbulence [89, 90].

We describe the structures of low-frequency SAW continuous spectrum in low β tokamak plasmas ($\beta = 8\pi P/B_0^2 \approx \epsilon^2$, with P the plasma pressure and B_0 the toroidal magnetic field on axis), taking into account both thermal plasma ion compressibility and diamagnetic effects, since experimental evidence and theoretical predictions show that this is important for the dynamics; thus, $\omega \approx \omega_{*pi} = (T_1 c/e_1 B^2)(\mathbf{k} \times \mathbf{B}) \cdot \nabla \ln P_1$, where ω_{*pi} is the thermal plasma ion diamagnetic frequency. SAW/SMW coupling is treated on the same footing of kinetic descriptions of both circulating as well as trapped particles, while finite Larmor radius (FLR) and finite magnetic drift orbit width (FOW) effects are neglected (see [12, 22, 49, 50] for analyses including FLR/FOW). In this paper we use a simplified model for circulating and trapped particles, considering the former as well circulating with constant velocity and the latter as deeply trapped, i.e. characterized by harmonic bounce motion between magnetic mirror points. Despite this assumption, the theoretical description presented here captures the essential qualitative features of the relevant wave–particle interactions and correctly reproduces functional forms of asymptotic limits at both low [83] and high [7] frequencies. A brief but general discussion of the reason why this is the case is given at the beginning of section 2. For the sake of simplicity, we also assume high poloidal mode numbers with kinetic singular layer at $k_{\parallel} q R_0 = 0$ [7]. This choice allows us to elucidate the important physics effects of trapped particles on the low-frequency structures of SAW continuous spectrum in toroidal geometry, while keeping technical difficulties to a minimum. For example, with the extended Λ expression of equation (24), it is possible to use equation (1) to describe BAE/BAAE mode excitations by either thermal (short wavelength) or fast ions (long wavelength) and to compute the SAW continuum structure by $\Lambda^2 = k_{\parallel}^2 q^2 R_0^2$, inclusive of diamagnetic, BAE and BAAE accumulation points. Note, once more, that this is the case for mode structures with kinetic singular layer at $k_{\parallel} q R_0 = 0$ and with either small diamagnetic effects or sufficiently high mode numbers that degeneracy removal between poloidal sidebands is unimportant. In a separate and more formal and general work, we will analyze the same problem considered here, in which both circulating and trapped particles are treated in action angle variables, with a realistic description of particle motion in the whole considered frequency range. In that work, unlike here, we will also consider the degeneracy removal between poloidal sidebands parallel wavevectors at finite $|k_{\parallel} q R_0|$ [28–30, 69] and/or between poloidal sideband diamagnetic effects at moderate or small poloidal mode number m [20, 29, 30].

This paper is organized as follows. In section 2, we present the kinetic theory of wave–particle interactions at low frequencies. There, we show how different treatments of circulating [7] and trapped particles (this work) can be combined in the present theoretical framework. Section 3 discusses the gyrokinetic equation solution for deeply trapped particles, using a coordinate transformation from guiding center to banana orbit center [5]. The quasi-neutrality equation is solved including both circulating and trapped particles. In section 4, the expression of Λ is derived, encompassing contributions for circulating and trapped particles.

The very low frequency and fluid limits are discussed in section 5, with a comparison of present with previous results in each limit. For the sake of completeness, the general derivation of asymptotic limiting cases at low ($|\omega| \ll \omega_{Bi}$ [83]) and high frequencies ($\omega_{Ti} \ll |\omega| \ll \omega_A$ [7]) is given in appendix A. Derivations of modified circulating thermal ion behaviors in the presence of finite trapped particle fraction are also given in appendix B. Preliminary numerical studies of analytic results are discussed in section 6, with the aim of elucidating the qualitative effect of trapped particles on the structure of the shear Alfvén continuous spectrum and on Alfvén Eigenmode frequencies. Concluding remarks are finally given in section 7.

2. Theoretical model

The main scope of this work—as discussed in the introduction—is to extend previous investigations of the inertial/kinetic layer response [7] and generalize the expression of Λ in equation (1) to $0 < |\omega| < \omega_{BAE}$ by inclusion of trapped particle dynamics [20, 29, 30]. Inertial/kinetic layer mode properties are intimately related to particle magnetic drifts [8] and can be understood as response to perpendicular (radial) and parallel electric field. Due to the sharply varying radial mode structures in the layer region, geodesic curvature particle drifts dominate perpendicular dynamics, in which wave–particle interactions enter only via precession-bounce (for trapped particles) and transit resonances (for circulating particles). This fact can be readily verified, since $\omega_{dg} = \mathbf{k} \cdot \mathbf{v}_{dg} = -i(v_{\parallel}/\omega_c) \nabla \times (\mathbf{b}v_{\parallel}) \cdot \nabla r \partial_r$, with \mathbf{v}_{dg} the geodesic particle magnetic drift velocity, v_{\parallel} the parallel (to \mathbf{B}) speed, $\omega_c = eB/(mc)$ the cyclotron frequency of a particle of charge e and mass m and $\mathbf{b} = \mathbf{B}/B$. We also employ straight magnetic field line toroidal coordinates (r, ϑ, ζ) , with r the radial-like flux coordinate, ϑ the poloidal angle and ζ the generalized toroidal coordinate chosen such that $q = \mathbf{B} \cdot \nabla \zeta / \mathbf{B} \cdot \nabla \vartheta = q(r)$. Thus,

$$\omega_{dg} = -i \frac{v_{\parallel} B}{\omega_c} \frac{\partial}{\partial \ell} \left(\frac{\mathbf{b} \cdot \nabla r \times \nabla \vartheta v_{\parallel}}{\mathbf{b} \cdot \nabla \vartheta B} \right) \frac{\partial}{\partial r},$$

where $\partial/\partial \ell = \mathbf{b} \cdot \nabla = (1/B)(\nabla \psi_p \times \nabla \vartheta \cdot \nabla \zeta) \partial/\partial \vartheta$ and ψ_p is the poloidal magnetic flux. From the last expression, it is evident that geodesic particle magnetic drifts do not enter bounce-averaged dynamics ($\oint d\ell/v_{\parallel}(\dots)$ on closed equilibrium particle orbits); i.e. perpendicular dynamics is dominated by ions, for they have larger characteristic orbit size, while electrons—with their fast bounce/transit motion ($|\omega| \ll \omega_{Be} < \omega_{Te}$)—respond as massless fluid to perpendicular ion charge separation [8] by sustaining a parallel electric field with periodic structure along the magnetic field lines to ensure overall charge neutrality. As further consequence of this argument, one readily concludes that wave–particle interactions via precession resonance in the layer region should enter via bounce-averaged dynamics, i.e. via the ‘flute-like’ component of the parallel electric field slowly varying along \mathbf{B} .

These conclusions are confirmed by the derivations reported in section 3, which apply to our present model equilibrium and simplified description of particle motions; however, they are generally valid for arbitrary equilibria and precise representation of particle orbits. For this reason, the results of this work capture the essential qualitative features of the relevant wave–particle interactions and correctly reproduce functional forms of asymptotic limits at both low [83] and high [7] frequencies, as anticipated in the introduction. The evident limitation of our analysis is due to the approximated description of the particle phases space, especially when the behavior of barely trapped/circulating particles becomes important. This is known to be the case, e.g., in the presence of strong pressure gradients (such as with internal transport barriers) and/or with negative or strong magnetic shear. In those conditions, theoretical results presented here should not be used in the precession frequency range and may be misleading since they

neglect important aspects of precession frequency dependence on local equilibrium parameters and could never account, e.g., for reversal of particle toroidal precession. These aspects will be more thoroughly addressed in a separate work, at the expense of a more complicated formal theoretical description.

In this work, we consider a low $\beta \approx \epsilon^2$ axisymmetric tokamak plasma equilibrium with shifted circular flux surfaces, where magnetic shear $s = rq'/q$ and $\alpha = -R_0 q^2 \beta'$ define a two-parameter set of plasma equilibria [91] and prime denotes derivation with respect to r . Furthermore, for the sake of simplicity as anticipated in section 1, we treat all trapped particles as deeply trapped (i.e. characterized by harmonic motion between magnetic mirror points) and consider circulating particles as well circulating (i.e. characterized by constant parallel velocity).

The plasma is described by three fluctuating scalar fields [92, 93]: the scalar potential perturbation $\delta\phi$, the perturbed parallel magnetic field δB_{\parallel} and the perturbed field $\delta\psi$, defined in terms of the parallel vector potential:

$$\delta A_{\parallel} = -i \left(\frac{c}{\omega} \right) \mathbf{b} \cdot \nabla \delta\psi.$$

With this representation, the parallel perturbed electric field is $\delta E_{\parallel} = -\mathbf{b} \cdot \nabla(\delta\phi - \delta\psi)$. The ideal magnetohydrodynamic (MHD) limit is obtained for $\delta E_{\parallel} = 0$, i.e. setting $\delta\phi = \delta\psi$.

The perturbed particle distribution function can be expressed as [92, 93]

$$\delta f_s = \left(\frac{e}{m} \right)_s \left[\frac{\partial f_0}{\partial \varepsilon} \delta\phi - J_0(k_{\perp} \rho_L) \frac{Q f_0}{\omega} e^{iL_k} \delta\psi \right]_s + e^{iL_{k_s}} \delta K_s,$$

where $s = i, e$ is the species index, e_s the electric charge, f_{0s} the equilibrium distribution function, $\varepsilon = v^2/2$ the energy per unit mass, J_0 the Bessel function of zero order, k_{\perp} the perpendicular (to \mathbf{b}) wave number, ρ_L the Larmor radius and $Q f_{0s} = (\omega \partial_{\varepsilon} + \hat{w}_{*})_s f_{0s}$, where $\hat{w}_{*s} f_{0s} = (m_s c / e_s B) (\mathbf{k} \times \mathbf{b}) \cdot \nabla f_{0s}$ and $L_{k_s} = (m_s c / e_s B) (\mathbf{k} \times \mathbf{b}) \cdot \mathbf{v}$.

In this paper we will closely follow the procedure presented in [7]. Adopting the ballooning formalism [91] in the space of the extended poloidal angle θ , the particle distribution function can be calculated from the gyrokinetic equation [93]

$$[v_{\parallel} \mathbf{b} \cdot \nabla - i(\omega - \omega_d)]_s \delta K_s = i(e_s / m_s) Q f_{0s} J_0(\lambda) \left[\frac{\omega_{ds}}{\omega} \delta\psi + (\delta\phi - \delta\psi) \right], \quad (2)$$

where $\lambda = k_{\perp} v_{\perp} / \omega_c$, $\omega_d = \mathbf{k} \cdot \mathbf{v}_d$ is the drift frequency and $\mathbf{v}_d = \mathbf{b} \times \mathbf{k} (\mu B + v_{\parallel}^2) / \omega_c$ the magnetic drift velocity. In equation (2), we have excluded the fast magneto-acoustic waves by assuming perpendicular pressure balance [8, 93]. Explicitly solving for δB_{\parallel} and using the plasma equilibrium condition, one can show that it is correct to ignore δB_{\parallel} provided that ∇B drift is substituted by curvature drift in the \mathbf{v}_d expression [8, 93].

The governing equations for the two fields $\delta\phi$ and $\delta\psi$ are the coupled vorticity equation and quasi-neutrality condition [92, 93]. The first one reads [5, 7]:

$$\begin{aligned} B \mathbf{b} \cdot \nabla \left[\frac{1}{B} \frac{k_{\perp}^2}{k_{\vartheta}^2} \mathbf{b} \cdot \nabla \delta\psi \right] + \frac{\omega^2}{v_A^2} \left(1 - \frac{\omega_{*pi}}{\omega} \right) \frac{k_{\perp}^2}{k_{\vartheta}^2} \delta\phi + \frac{\alpha}{q^2 R^2} g(\theta) \delta\psi \\ = \left\langle \sum_s \frac{4\pi e_s}{k_{\vartheta}^2 c^2} J_0(k_{\perp} \rho_{L_s}) \omega \omega_{ds} \delta K_s \right\rangle, \end{aligned} \quad (3)$$

where $\langle \dots \rangle = \int d\mathbf{v}(\dots)$ denotes integration in velocity space, $\mathbf{b} \cdot \nabla = (qR_0)^{-1} \partial_{\theta}$, $k_{\perp}^2 / k_{\vartheta}^2 = 1 + k_r^2 / k_{\vartheta}^2 = 1 + (s\theta - \alpha \sin \theta)^2$, k_r and k_{ϑ} are radial and poloidal wave-numbers, respectively, $g(\theta) = \cos \theta + [s\theta - \alpha \sin \theta] \sin \theta$, $\omega_{*ps} = \omega_{*ns} + \omega_{*Ts}$, $\omega_{*ns} = (T_s c / e_s B) (\mathbf{k} \times \mathbf{b}) \cdot \nabla (n_s) / n_s$, $\omega_{*Ts} = (T_s c / e_s B) (\mathbf{k} \times \mathbf{b}) \cdot \nabla (T_s) / T_s$ and n_s is the

species' particle density. Meanwhile, the quasi-neutrality condition can be put in the following form:

$$\left(1 + \frac{1}{\tau}\right) (\delta\phi - \delta\psi) + \left(1 - \frac{\omega_{*pi}}{\omega}\right) b_i \delta\psi = \frac{T_i}{ne} (J_0(k_\perp \rho_{Li}) \delta K_i - \delta K_e), \quad (4)$$

where $\tau = T_e/T_i$, $b_i = k_\perp^2 (m_i c^2 T_i / e^2 B^2)$ and $n = n_e = n_i$. In equation (3), \sum_s is generally extended to all ion species (thermal and energetic); however, we limit our present treatment to one thermal ion species only with unit electric charge. Meanwhile, neglecting FLR/FOW corresponds to taking $J_0(k_\perp \rho_{Li}) = 1$ and $b_i = 0$ in equations (3) and (4).

Given the coupled system of equations (3) and (4), equation (1) is obtained by asymptotic matching of kinetic (inertial) layer and ideal region solutions. The kinetic layer is characterized by sharply varying radial structures, with $k_\perp^2/k_\theta^2 \gg 1$ or, equivalently $s^2|\theta|^2 \gg 1$. For $|s| = O(1)$, the kinetic layer corresponds to $|\theta| = O(\beta^{-1/2})$, since the optimal frequency ordering $|k_\parallel|v_A \approx \omega_{Ti}$ implies $|k_\parallel|qR_0 \approx |\theta|^{-1} \approx \beta^{1/2}$ [7], with k_\parallel the parallel (to \mathbf{b}) wave vector. For large $|\theta| = O(\beta^{-1/2})$, the fluctuating fields show a two-scale behavior: they vary on a short scale $\theta_0 \approx 1$ and on a long scale $\theta_1 \approx O(\beta^{-1/2})$. For convenience, we will work with the rescaled potentials $\delta\Phi = (k_\perp/k_\theta)\delta\phi$ and $\delta\Psi = (k_\perp/k_\theta)\delta\psi$, and represent them both as asymptotic series in powers of $\beta^{1/2}$; e.g., $\delta\Phi = \delta\Phi^{(0)} + \delta\Phi^{(1)} + \delta\Phi^{(2)} + \dots$, where $\delta\Phi^{(1)} = O(\beta^{1/2})$, $\delta\Phi^{(2)} = O(\beta)$, etc.

The asymptotic expansion in powers of $\beta^{1/2}$ is strictly applicable for circulating particles and the optimal frequency ordering $\omega \approx \omega_{*pi} \approx \omega_{Ti}$ [7]. At lower frequencies and when trapped particles are considered, this ordering changes and depends on the considered frequency range. Nonetheless, the asymptotic approach remains valid provided that the two-scale behavior of the fluctuating fields is preserved and $|\theta_1/\theta_0| \gg 1$. Then, strictly speaking, the asymptotic series is to be intended formally as an expansion in the smallness parameter θ_0/θ_1 . The actual scaling of this parameter with the physical quantities of the system can be obtained *a posteriori*, although a generic ordering can be obtained assuming $|k_\parallel|v_A \approx |\omega|$, yielding $|\theta_1/\theta_0| \approx |\omega_A/\omega| \gg 1$. Determining the kinetic (inertial) layer contribution $\propto \Lambda$ in equation (1) corresponds to reducing the coupled equation (3) and (4) to the form

$$(\partial_{\theta_1}^2 + \Lambda^2) \delta\Psi^{(0)} = 0,$$

as demonstrated in section 4. As a first step towards showing this, in section 3 we solve the gyrokinetic equation equation (2) for deeply trapped particles.

3. Solutions of the gyrokinetic equation

In this section, we solve equation (2) for deeply trapped particles: the solution for well circulating particles can be found in [7].

For large aspect ratio tokamaks $\epsilon \ll 1$ and thus the magnetic field is $B \approx B_0(1 - \epsilon \cos \theta)$. The parallel velocity is then $v_\parallel^2 = 2[\epsilon - \mu B_0(1 - \epsilon \cos \theta)]$. Since we treat all trapped particles as deeply trapped, the latter equation can be written as $v_\parallel = \theta_b \omega_b q R_0 \cos \eta$, where $\theta_b^2 = 2[\epsilon - \mu B_0(1 - \epsilon)]/\epsilon \mu B_0$ is the particle bounce angle ($\theta = \pm \theta_b$ defines the magnetic mirror points), and $\omega_b = (\epsilon \mu B_0)^{1/2}/q R_0$ is the particle bounce frequency. For deeply trapped particles, we have introduced the notation $\theta_0 = \theta_b \sin \eta$, where η is the phase angle of harmonic oscillations on the banana orbit and θ_0 is the fast variation scale of the mode structures (see section 2). Thus, for deeply trapped particles we have $\omega_d = \bar{\omega}_d(1 + \xi \theta_b \sin \eta)$, where $\xi = (i/nq)r\partial/\partial r = -(r/nq)k_r \approx \theta_1$. For consistency of our two-scale asymptotic approach (see section 2), we assume $\theta_b \approx \theta_0/\theta_1$, so that $\xi \theta_b \approx 1$ when considering the kinetic (inertial)

layer. Moving to the banana orbit center frame [5, 94]

$$\delta K = \exp\left(i\frac{\bar{\omega}_d}{\omega_b}\xi\theta_b \cos \eta\right) \delta K_b = (\Sigma_h i^h J_h(\lambda_b) e^{-i\eta h}) \delta K_b. \quad (5)$$

Here, δK_b is the particle distribution function in the banana orbit center reference frame, $\lambda_b = \theta_b(\bar{\omega}_d/\omega_b)\xi$, and $J_h(\lambda_b)$ are Bessel functions. For small banana width, $\lambda_b \ll 1$, and we can approximate $J_0(\lambda_b) \approx 1$ and $J_1(\lambda_b) \approx \lambda_b/2$. Meanwhile, $v_{\parallel}\partial/\partial\ell = \omega_b\partial/\partial\eta$ for deeply trapped particles and thus

$$\begin{aligned} [\omega_b\partial_{\eta} - i(\omega - \bar{\omega}_d)]\delta K_b &= i\frac{e}{m}Qf_0\Sigma_h(-i)^h e^{i\eta h} J_0(\lambda) J_h(\lambda_b) \\ &\times \frac{k_{\vartheta}}{k_{\perp}} \left[\delta\Phi - \delta\Psi + \frac{\bar{\omega}_d}{\omega}(1 + \xi\theta_b \sin \eta)\delta\Psi \right]. \end{aligned}$$

The latter equation is an ordinary differential equation in η space, which is solved by expanding $\delta\Psi = \delta\Psi^{(0)} + \delta\Psi^{(1)}$ and $\delta\Phi = \delta\Phi^{(0)} + \delta\Phi^{(1)}$. It is easy to show that $\delta\Psi^{(0)} = \delta\Psi^{(0)}(\theta_1)$ and $\delta\Psi^{(1)} = 0$, using the vorticity equation [7]. Following [7], we also know that—for $\omega \approx \omega_{*pi} \approx \omega_{Ti}$ —the lowest order solution for $\delta\Phi$ is $\delta\Phi^{(0)} = \delta\Psi^{(0)}(\theta_1)$; meanwhile, using the fact that $\omega_{di}/\omega_{Ti} \approx \theta_0/\theta_1$, $\delta\Phi^{(1)} = \delta\Phi_s(\theta_1) \sin \theta_0 + \delta\Phi_c(\theta_1) \cos \theta_0 \simeq \delta\Phi_s(\theta_1) \sin \theta_0$, where $\delta\Phi_s(\theta_1)$ and $\delta\Phi_c(\theta_1)$ vary only on a long scale θ_1 and $\delta\Phi_s(\theta_1) \approx \xi\delta\Phi_c(\theta_1)$, hence $|\delta\Phi_s(\theta_1)| \gg |\delta\Phi_c(\theta_1)|$. Since we consider only deeply trapped particles ($\cos \theta_0 \approx 1$ and $\sin \theta_0 \approx \theta_0$), we can write $\delta\Phi^{(1)} = \delta\Phi_s\theta_b \sin \eta$. At lower frequencies and when deeply trapped particles are included, direct inspection of equations (3) and (4) shows that one can still assume $\delta\Phi \simeq \delta\Phi^{(0)}(\theta_1) + \delta\Phi_s(\theta_1) \sin \theta_0$, where now $\delta\Phi_s \approx \delta\Phi^{(0)}$ at $\omega \approx \omega_{di}$. That this solution satisfies equations (3) and (4) can also be verified *a posteriori*. Thus, our asymptotic approach can be used in the whole frequency range $0 < |\omega| \ll \omega_A$.

Because the trapped particle fraction is of order $\epsilon^{1/2}$ and $\lambda_b \ll 1$, equation (5) at lowest and relevant order gives $\delta K \simeq \delta K_b$. Recalling that ω_{be} is very large, we find that the fluctuating electron response is given by the bounce-averaged response

$$\delta K_e = -Qf_{0e} \left(\frac{e}{m}\right)_e \frac{k_{\vartheta}/k_{\perp}}{\omega - \bar{\omega}_{de}} \left[\frac{\bar{\omega}_{de}}{\omega} \delta\Psi^{(0)} + \delta\Phi^{(0)} - \delta\Psi^{(0)} \right] \quad (6)$$

as long as finite electron inertia is neglected consistently, considering sufficiently long space-scales (see [74] for a more detailed discussion of this effect). Meanwhile, the trapped thermal ion response is obtained in the following form:

$$\begin{aligned} \delta K_i &= -Qf_{0i} \left(\frac{e}{m}\right)_i \frac{k_{\vartheta}/k_{\perp}}{\omega - \bar{\omega}_{di}} \left[\frac{\bar{\omega}_{di}}{\omega} \delta\Psi^{(0)} + \delta\Phi^{(0)} - \delta\Psi^{(0)} \right] \\ &- Qf_{0i} \left(\frac{e}{m}\right)_i \frac{k_{\vartheta}/k_{\perp}}{(\omega - \bar{\omega}_{di})^2 - \omega_b^2} [\bar{\omega}_{di}\xi\delta\Phi^{(0)} + (\omega - \bar{\omega}_{di})\delta\Phi_s] \sin \theta. \end{aligned} \quad (7)$$

In equation (7) we have omitted all odd terms in velocity space, since they will cancel in the upcoming integrations. Substituting these expressions in the quasi-neutrality equation and separating the sinusoidal and constant ('flute-like') terms, we arrive at

$$\begin{aligned} \left(1 + \frac{1}{\tau}\right) (\delta\Phi^{(0)} - \delta\Psi^{(0)}) &= \frac{T_i}{eN_i} \left\langle Qf_{0e} \left(\frac{e}{m}\right)_e \frac{1}{\omega - \bar{\omega}_{de}} \left(\frac{\bar{\omega}_{de}}{\omega} \delta\Psi^{(0)} + \delta\Phi^{(0)} - \delta\Psi^{(0)} \right) \right\rangle_{\text{tra}} \\ &\times \frac{T_i}{eN_i} \left\langle -Qf_{0i} \left(\frac{e}{m}\right)_i \frac{1}{\omega - \bar{\omega}_{di}} \left(\frac{\bar{\omega}_{di}}{\omega} \delta\Psi^{(0)} + \delta\Phi^{(0)} - \delta\Psi^{(0)} \right) \right\rangle_{\text{tra}} \\ &+ \frac{T_i}{eN_i} \left\langle -\frac{Qf_{0i}}{\omega} \left(\frac{e}{m}\right)_i (\delta\Phi^{(0)} - \delta\Psi^{(0)}) \right\rangle_{\text{cir}} \end{aligned} \quad (8)$$

and

$$\left(1 + \frac{1}{\tau}\right) \delta\Phi_s = \frac{T_i}{eN_i} \left\langle -Qf_{0i} \left(\frac{e}{m}\right)_i \frac{1}{(\omega - \bar{\omega}_{di})^2 - \omega_{bi}^2} (\bar{\omega}_{di}\xi \delta\Phi^{(0)} + (\omega - \bar{\omega}_{di})\delta\Phi_s) \right\rangle_{\text{tra}} \\ + \frac{T_i}{eN_i} \left\langle -Qf_{0i} \left(\frac{e}{m}\right)_i \frac{1}{\omega^2 - \omega_{ci}^2} (\bar{\omega}_{di}\xi \delta\Phi^{(0)} + \omega\delta\Phi_s) \right\rangle_{\text{cir}}, \quad (9)$$

where $\delta K_i^{(0)}$ and $\delta K_i^{(1)}$ for circulating particles are extracted from the particle response as follows [7]:

$$\delta K_{i,\text{cir}}^{(0)} = -\left(\frac{e}{m}\right)_i \frac{Qf_{0i}}{\omega} \frac{k_{\parallel}}{k_{\perp}} (\delta\Phi^{(0)} - \delta\Psi^{(0)}) \quad (10)$$

and

$$\delta K_{i,\text{cir}}^{(1)} = -\left(\frac{e}{m}\right)_i Qf_{0i} \frac{1}{\omega^2 - \omega_{ci}^2} \frac{k_{\parallel}}{k_{\perp}} (\bar{\omega}_{di}\xi \delta\Phi^{(0)} + \omega\delta\Phi_s) \sin\theta_0. \quad (11)$$

We first consider trapped particle velocity space integrations in equations (8) and (9). For trapped particles the integration in the velocity space can be written as

$$\langle(\dots)\rangle_{\text{tra}} = 2\pi \sum_{\sigma=\pm 1} \int_0^{\infty} d\varepsilon \int_{\varepsilon/B_{\text{max}}}^{\varepsilon/B} \frac{B}{|v_{\parallel}|} (\dots) d\mu,$$

with $B_{\text{max}} = B_0(1 + \epsilon)$ the maximum magnetic field value on the flux surface, while $B_{\text{min}} = B_0(1 - \epsilon)$. Since equations (6) and (7) do not explicitly depend on θ_b , for deeply trapped particles we can approximately write (see appendix A)

$$\langle(\dots)\rangle_{\text{tra}} \simeq 8\pi\epsilon^{1/2} \int_0^{\infty} \varepsilon^{1/2} d\varepsilon \cos(\theta/2) (\dots) \simeq 8\pi\epsilon^{1/2} \int_0^{\infty} \varepsilon^{1/2} d\varepsilon (\dots).$$

We also note that in equation (9) $\theta \cos(\theta/2) \simeq \sin\theta$ has been consistently assumed for deeply trapped particles. To proceed further, we assume a Maxwellian distribution function $f_{0s} = N_s/(2\pi\varepsilon_{Ts})^{3/2} e^{-\varepsilon/\varepsilon_{Ts}}$, for $s = i, e$, where we have denoted with $N_s = n$ the particle density and $\varepsilon_{Ts} = T_s/m_s$ the thermal energy of each species. Then equation (8) can be readily solved, leading to

$$\left(1 + \frac{1}{\tau}\right) (\delta\Phi^{(0)} - \delta\Psi^{(0)}) = \left(1 - \sqrt{2\epsilon}\right) \left(1 - \frac{\omega_{*ni}}{\omega}\right) (\delta\Phi^{(0)} - \delta\Psi^{(0)}) \\ + \sqrt{2\epsilon} \left[M\left(\frac{\omega}{\bar{\omega}_{Di}}\right) + \frac{1}{\tau} M\left(\frac{\omega}{\bar{\omega}_{De}}\right) \right] (\delta\Phi^{(0)} - \delta\Psi^{(0)}) \\ + \sqrt{2\epsilon} \left[L\left(\frac{\omega}{\bar{\omega}_{Di}}\right) + \frac{1}{\tau} L\left(\frac{\omega}{\bar{\omega}_{De}}\right) \right] \delta\Psi^{(0)}, \quad (12)$$

where

$$M\left(\frac{\omega}{\bar{\omega}_{Di}}\right) = -2 \frac{\omega}{\bar{\omega}_{Di}} \left\{ \left(1 - \frac{\omega_{*ni}}{\omega} + \frac{3}{2} \frac{\omega_{*Ti}}{\omega}\right) \left[1 + \sqrt{\frac{\omega}{\bar{\omega}_{Di}}} Z\left(\sqrt{\frac{\omega}{\bar{\omega}_{Di}}}\right)\right] \right. \\ \left. - \frac{\omega_{*Ti}}{\omega} \left[\frac{1}{2} + \frac{\omega}{\bar{\omega}_{Di}} + \left(\frac{\omega}{\bar{\omega}_{Di}}\right)^{3/2} Z\left(\sqrt{\frac{\omega}{\bar{\omega}_{Di}}}\right)\right] \right\} \quad (13)$$

and

$$L\left(\frac{\omega}{\bar{\omega}_{Di}}\right) = -2 \left\{ \left(1 - \frac{\omega_{*ni}}{\omega} + \frac{3}{2} \frac{\omega_{*Ti}}{\omega}\right) \left[\frac{1}{2} + \frac{\omega}{\bar{\omega}_{Di}} + \left(\frac{\omega}{\bar{\omega}_{Di}}\right)^{3/2} Z\left(\sqrt{\frac{\omega}{\bar{\omega}_{Di}}}\right)\right] \right. \\ \left. - \frac{\omega_{*Ti}}{\omega} \left[\frac{3}{4} + \frac{1}{2} \frac{\omega}{\bar{\omega}_{Di}} + \left(\frac{\omega}{\bar{\omega}_{Di}}\right)^2 + \left(\frac{\omega}{\bar{\omega}_{Di}}\right)^{5/2} Z\left(\sqrt{\frac{\omega}{\bar{\omega}_{Di}}}\right)\right] \right\} \quad (14)$$

with $Z(x) = 1/\sqrt{\pi} \int_{-\infty}^{\infty} e^{-y^2}/(y-x) dy$, while $M(\omega/\bar{\omega}_{De})$ and $L(\omega/\bar{\omega}_{De})$ are obtained from equations (13) and (14) by substitution $\bar{\omega}_{Di}, \omega_{*ni}, \omega_{*Ti} \rightarrow \bar{\omega}_{De}, \omega_{*ne}, \omega_{*Te}$. The normalization factor $(1-\sqrt{2}\epsilon)$ in equation (12), accounts for the reduced circulating particle population in the presence of trapped particles (see appendix B). Expanding the Z function for $|\omega| \gg |\bar{\omega}_{Di}|$, we obtain $M(\omega/\bar{\omega}_{Di}) \rightarrow (1-\omega_{*ni}/\omega)$, while $L(\omega/\bar{\omega}_{Di})$ tends to 0 as $\bar{\omega}_{Di}/\omega$. Thus equation (12) reduces to

$$\left(1 + \frac{1}{\tau}\right) (\delta\Phi^{(0)} - \delta\Psi^{(0)}) = \left(1 - \frac{\omega_{*ni}}{\omega}\right) (\delta\Phi^{(0)} - \delta\Psi^{(0)}).$$

This is the same result obtained by Zonca and Chen [7], for circulating particles only, and gives the solution $\delta\Phi^{(0)} = \delta\Psi^{(0)}$ which is the MHD limit of the theory, describing the plasma as a perfect conductor with vanishing parallel electric field. In general we can write $\delta\Phi^{(0)} = I_{\Phi}(\omega/\bar{\omega}_{Di}, \omega/\bar{\omega}_{De})\delta\Psi^{(0)}$, with

$$I_{\Phi}\left(\frac{\omega}{\bar{\omega}_{Di}}, \frac{\omega}{\bar{\omega}_{De}}\right) = 1 + \frac{\sqrt{2}\epsilon\tau (L(\omega/\bar{\omega}_{Di}) + \tau^{-1}L(\omega/\bar{\omega}_{De}))}{1 + \tau\omega_{*ni}/\omega + \sqrt{2}\epsilon\tau [1 - \omega_{*ni}/\omega - M(\omega/\bar{\omega}_{Di}) - \tau^{-1}M(\omega/\bar{\omega}_{De})]} \quad (15)$$

describing the non-vanishing ‘flute-like’ component of the parallel electric field due to the effect of trapped thermal particle precession resonance, which becomes negligibly small for $|\omega| \gg |\bar{\omega}_{Di}|, |\bar{\omega}_{De}|$. As we will demonstrate in the following and consistently with the discussion at the beginning of section 2, $I_{\Phi}(\omega/\bar{\omega}_{Di}, \omega/\bar{\omega}_{De})$ defined in equation (15) describes the only process through which thermal particle precession resonance can directly affect the kinetic layer response, which is otherwise dominated by geodesic curvature couplings, depending on thermal ion precession-bounce or transit resonances. This effect is generally small for $|\omega| \gg |\bar{\omega}_{Di}|, |\bar{\omega}_{De}|$ and it is possible to consider $I_{\Phi}(\omega/\bar{\omega}_{Di}, \omega/\bar{\omega}_{De}) \simeq 1$ for a non-vanishing denominator in equation (15).

Equation (9) is more difficult to solve since both the precession and the bounce frequency are functions of the energy of the particles: $\bar{\omega}_d \propto \epsilon$, and $\omega_b \propto \epsilon^{1/2}$. The integrals coming from angular brackets have the following form:

$$G_n = \frac{1}{\pi^{1/2}} \int_{-\infty}^{\infty} \frac{e^{-x^2} x^n}{(\omega/\bar{\omega}_{Di} - x^2)^2 - (\omega_{Bi}/\bar{\omega}_{Di})^2 x^2} dx,$$

for $n = 2, 4, 6, 8$. Note that, here, we have made explicit all dependences on $\bar{\omega}_{Di}$ and ω_{Bi} as the deeply trapped ion thermal precession and bounce frequencies. In order to evaluate these integrals we introduce

$$\Omega_1 = \frac{\frac{\omega_{Bi}}{\bar{\omega}_{Di}} + \sqrt{\left(\frac{\omega_{Bi}}{\bar{\omega}_{Di}}\right)^2 + 4\frac{\omega}{\bar{\omega}_{Di}}}}{2}$$

and

$$\Omega_2 = \frac{-\frac{\omega_{Bi}}{\bar{\omega}_{Di}} + \sqrt{\left(\frac{\omega_{Bi}}{\bar{\omega}_{Di}}\right)^2 + 4\frac{\omega}{\bar{\omega}_{Di}}}}{2}.$$

The G_n integrals have the following functional forms:

$$G_2 = \frac{\bar{\omega}_{Di}/\omega_{Bi}}{\Omega_1 + \Omega_2} [\Omega_1 Z(\Omega_1) - \Omega_2 Z(\Omega_2)],$$

$$G_4 = \frac{\bar{\omega}_{Di}/\omega_{Bi}}{\Omega_1 + \Omega_2} [\Omega_1^2 - \Omega_2^2 + \Omega_1^3 Z(\Omega_1) - \Omega_2^3 Z(\Omega_2)],$$

$$G_6 = \frac{\bar{\omega}_{\text{Di}}/\omega_{\text{Bi}}}{\Omega_1 + \Omega_2} \left[(1/2)(\Omega_1^2 - \Omega_2^2) + \Omega_1^4 - \Omega_2^4 + \Omega_1^5 Z(\Omega_1) - \Omega_2^5 Z(\Omega_2) \right],$$

$$G_8 = \frac{\bar{\omega}_{\text{Di}}/\omega_{\text{Bi}}}{\Omega_1 + \Omega_2} \left[(3/4)(\Omega_1^2 - \Omega_2^2) + (1/2)(\Omega_1^4 - \Omega_2^4) + \Omega_1^6 - \Omega_2^6 + \Omega_1^7 Z(\Omega_1) - \Omega_2^7 Z(\Omega_2) \right].$$

Finally equation (9) gives:

$$\delta\Phi_s = - \frac{N_1 \left(\frac{\omega}{\omega_{\text{Ti}}} \right) + \Delta N_1 \left(\frac{\omega}{\omega_{\text{Ti}}} \right) + \sqrt{2\epsilon} P_2 \left(\frac{\omega}{\bar{\omega}_{\text{Di}}}, \frac{\omega_{\text{Bi}}}{\bar{\omega}_{\text{Di}}} \right)}{1 + \frac{1}{\tau} + D_1 \left(\frac{\omega}{\omega_{\text{Ti}}} \right) + \Delta D_1 \left(\frac{\omega}{\omega_{\text{Ti}}} \right) + \sqrt{2\epsilon} \left[P_1 \left(\frac{\omega}{\bar{\omega}_{\text{Di}}}, \frac{\omega_{\text{Bi}}}{\bar{\omega}_{\text{Di}}} \right) - P_2 \left(\frac{\omega}{\bar{\omega}_{\text{Di}}}, \frac{\omega_{\text{Bi}}}{\bar{\omega}_{\text{Di}}} \right) \right]} \xi \delta\Phi^{(0)}, \quad (16)$$

where $P_1(\omega/\bar{\omega}_{\text{Di}}, \omega_{\text{Bi}}/\bar{\omega}_{\text{Di}})$ and $P_2(\omega/\bar{\omega}_{\text{Di}}, \omega_{\text{Bi}}/\bar{\omega}_{\text{Di}})$ come from the trapped particles dynamics and can be calculated as

$$P_1(\omega/\bar{\omega}_{\text{Di}}, \omega_{\text{Bi}}/\bar{\omega}_{\text{Di}}) = -2 \frac{\omega^2}{\bar{\omega}_{\text{Di}}^2} \left[\left(1 - \frac{\omega_{*n}}{\omega} + \frac{3}{2} \frac{\omega_{*T}}{\omega} \right) G_2 - \frac{\omega_{*T}}{\omega} G_4 \right],$$

$$P_2(\omega/\bar{\omega}_{\text{Di}}, \omega_{\text{Bi}}/\bar{\omega}_{\text{Di}}) = -2 \frac{\omega}{\bar{\omega}_{\text{Di}}} \left[\left(1 - \frac{\omega_{*n}}{\omega} + \frac{3}{2} \frac{\omega_{*T}}{\omega} \right) G_4 - \frac{\omega_{*T}}{\omega} G_6 \right].$$

On the other hand, the functions

$$D_1(x) = x \left(1 - \frac{\omega_{*ni}}{\omega} \right) Z(x) - \frac{\omega_{*Ti}}{\omega} x [x + (x^2 - 1/2)Z(x)] \quad (17)$$

and

$$N_1(x) = 2(\bar{\omega}_{\text{Di}}/\omega_{\text{Ti}})N(x),$$

where

$$N(x) = \left(1 - \frac{\omega_{*ni}}{\omega} \right) [x + (1/2 + x^2)Z(x)] - \frac{\omega_{*Ti}}{\omega} [x(1/2 + x^2) + (1/4 + x^4)Z(x)], \quad (18)$$

come from the circulating particles dynamics [7]. Meanwhile, the functions $\Delta N_1(x)$ and $\Delta D_1(x)$ account for circulating particle dynamic modification due to finite trapped particle fraction; in [appendix B](#), it is shown that they are given by

$$\Delta D_1(x) = \frac{x}{\pi^{1/2}} \int_0^\infty e^{-y} \ln \left(\frac{x + \sqrt{2\epsilon y}}{x - \sqrt{2\epsilon y}} \right) \left[1 - \frac{\omega_{*ni}}{\omega} - \frac{\omega_{*Ti}}{\omega} \left(y - \frac{3}{2} \right) \right] dy, \quad (19)$$

$$\Delta N_1(x) = \frac{\bar{\omega}_{\text{Di}}/\omega_{\text{Ti}}}{\pi^{1/2}} \int_0^\infty y e^{-y} \ln \left(\frac{x + \sqrt{2\epsilon y}}{x - \sqrt{2\epsilon y}} \right) \left[1 - \frac{\omega_{*ni}}{\omega} - \frac{\omega_{*Ti}}{\omega} \left(y - \frac{3}{2} \right) \right] dy. \quad (20)$$

For brevity, from now on we will use the notation $\delta\Phi_s = S(\omega, \bar{\omega}_{\text{Di}}, \omega_{\text{Bi}}, \omega_{\text{Ti}}) \xi \delta\Phi^{(0)}$ to indicate the relation in equation (16).

4. Kinetic layer wave equation and expression of Λ

Following [7], we find the vorticity equation at second order in the asymptotic expansion in the form:

$$\frac{\partial^2}{\partial \theta_0^2} \delta\Psi^{(2)} + \frac{\partial^2}{\partial \theta_1^2} \delta\Psi^{(0)} + \frac{\omega^2}{\omega_A^2} \left(1 - \frac{\omega_{*pi}}{\omega} \right) \delta\Phi^{(0)} = \sum_s \frac{k_\parallel}{k_\perp} \left\langle \frac{4\pi\omega e_s}{k_\perp^2 c^2} q^2 R_0^2 \omega_{ds} \delta K_s \right\rangle.$$

The integration within the brackets can be separated in circulating and trapped particles velocity space:

$$\langle \omega_d \delta K \rangle = \langle \omega_d \delta K \rangle_{\text{cir}} + \langle \omega_d \delta K \rangle_{\text{tra}}.$$

Keeping only the constant ('flute-like') term in the equation, we obtain

$$\frac{\partial^2}{\partial \theta_1^2} \delta \Psi^{(0)} + \frac{\omega^2}{\omega_A^2} \left(1 - \frac{\omega_{*pi}}{\omega}\right) I_\Phi \delta \Psi^{(0)} + \Lambda_{\text{cir}}^2 I_\Phi \delta \Psi^{(0)} = \sum_s \frac{4\pi e_s}{k_\perp^2 c^2} q^2 R_0^2 \overline{\langle \omega \omega_{ds} (k_\perp / k_\vartheta) \delta K_s \rangle}_{\text{tra}},$$

where

$$\begin{aligned} \Lambda_{\text{cir}}^2 = q^2 \frac{\omega \omega_{Ti}}{\omega_A^2} & \left[\left(1 - \frac{\omega_{*ni}}{\omega}\right) \left(F\left(\frac{\omega}{\omega_{Ti}}\right) + \Delta F\left(\frac{\omega}{\omega_{Ti}}\right) \right) - \frac{\omega_{*Ti}}{\omega} \left(G\left(\frac{\omega}{\omega_{Ti}}\right) \right. \right. \\ & \left. \left. + \Delta G\left(\frac{\omega}{\omega_{Ti}}\right) \right) + \frac{\omega \omega_{Ti}}{4\bar{\omega}_{Di}^2} \left(N_1\left(\frac{\omega}{\omega_{Ti}}\right) + \Delta N_1\left(\frac{\omega}{\omega_{Ti}}\right) \right) S(\omega, \bar{\omega}_{Di}, \omega_{Bi}, \omega_{Ti}) \right] \\ & \xrightarrow{\text{circ. only}} q^2 \frac{\omega \omega_{Ti}}{\omega_A^2} \left[\left(1 - \frac{\omega_{*ni}}{\omega}\right) F(\omega/\omega_{Ti}) - \frac{\omega_{*Ti}}{\omega} G(\omega/\omega_{Ti}) - \frac{N^2(\omega/\omega_{Ti})}{D(\omega/\omega_{Ti})} \right] \end{aligned}$$

reduces to the circulating particle response as calculated by Zonca and Chen [7]. The functions within the brackets are:

$$F(x) = x(x^2 + 3/2) + (x^4 + x^2 + 1/2) Z(x),$$

$$G(x) = x(x^4 + x^2 + 2) + (x^6 + x^4/2 + x^2 + 3/4) Z(x),$$

$$D(x) = \left(\frac{1}{x}\right) \left(1 + \frac{T_i}{T_e}\right) + \left(1 - \frac{\omega_{*ni}}{\omega}\right) Z(x) - \frac{\omega_{*Ti}}{\omega} [x + (x^2 - 1/2) Z(x)], \quad (21)$$

while $N(x)$ is given by equation (18) and $\Delta F(\omega/\omega_{Ti})$ and $\Delta G(\omega/\omega_{Ti})$ describe, as for equations (19) and (20), the circulating particle dynamic modification due to finite trapped particle fraction (see appendix B):

$$\Delta F(x) = \frac{1}{\pi^{1/2}} \int_0^\infty e^{-y} \ln \left(\frac{x + \sqrt{2\epsilon y}}{x - \sqrt{2\epsilon y}} \right) \frac{y^2}{4} dy, \quad (22)$$

$$\Delta G(x) = \frac{1}{\pi^{1/2}} \int_0^\infty e^{-y} \ln \left(\frac{x + \sqrt{2\epsilon y}}{x - \sqrt{2\epsilon y}} \right) \frac{y^2}{4} \left(y - \frac{3}{2}\right) dy. \quad (23)$$

Since the kinetic layer wave equation is in the form $(\partial^2/\partial \theta_1^2) \delta \Psi^{(0)} + \Lambda^2 \delta \Psi^{(0)} = 0$, the general expression of Λ^2 can be written as

$$\Lambda^2/I_\Phi = \frac{\omega^2}{\omega_A^2} \left(1 - \frac{\omega_{*pi}}{\omega}\right) + \Lambda_{\text{cir}}^2 + \Lambda_{\text{tra}}^2,$$

where $\Lambda_{\text{tra}}^2 \delta \Phi^{(0)} = -\sum_s (4\pi e_s)/(k_\perp^2 c^2) q^2 R_0^2 \overline{\langle \omega \omega_{ds} (k_\perp / k_\vartheta) \delta K_s \rangle}_{\text{tra}}$ is the trapped particle contribution only and the bar denotes 'flux surface averaging'.

We note that Λ_{tra}^2 contains the factor $1/k_\perp^2$. In the inertial layer region, $|k_\perp/k_\vartheta|$ has a large value and only the terms containing $\xi^2 = k_r^2/k_\vartheta^2$ will contribute to the final result since in this region $k_\perp \approx k_r$. The $\delta \Phi_s$ term in equation (7) is proportional to ξ so this term will enter the final relation. On the other hand, terms proportional to $1/(\omega - \bar{\omega}_d)$ in equations (6) and (7) will not contribute for either electrons or for ions. Hence, we conclude that there are no precession frequency resonance effects and no electron contributions in the layer region, other than those discussed in connection with equation (15). Electron dynamics enters via the $\tau = T_e/T_i$ factor in the quasi-neutrality equation, which describes the electron response to the ion motion. The fact that only terms containing $\xi = k_r/k_\vartheta$ contribute to the kinetic (inertial) layer physics shows that the general response is related to the drift velocity modulation due to the geodesic curvature, while the normal curvature effects appear solely in the ideal region or via I_Φ . These considerations lead to the following final form of Λ^2 :

$$\Lambda^2/I_\Phi = \frac{\omega^2}{\omega_A^2} \left(1 - \frac{\omega_{*pi}}{\omega}\right) + \Lambda_{\text{cir}}^2 + \frac{\omega^2 \omega_{Bi}^2}{\omega_A^2 \bar{\omega}_{Di}^2} \frac{q^2}{\sqrt{2\epsilon}} [P_3 + (P_2 - P_3) S(\omega, \bar{\omega}_{Di}, \omega_{Bi}, \omega_{Ti})], \quad (24)$$

where

$$P_3 = -2 \left[\left(1 - \frac{\omega_{*n}}{\omega} + \frac{3}{2} \frac{\omega_{*T}}{\omega} \right) G_6 - \frac{\omega_{*T}}{\omega} G_8 \right].$$

This expression can be used in the general fishbone-like dispersion relation, equation (1), for describing a variety of shear Alfvén modes in a wide frequency range, from 0 to ω_{BAE} . Note that equation (24), similarly to equation (15), is valid up to $O(\epsilon^{1/2})$ with respect to the leading order, for consistency of our asymptotic approach. For low toroidal numbers and/or finite $k_{\parallel}qR_0$, we also need to consider the degeneracy removal between poloidal sidebands (see section 1). The drawback of this dispersion relation is that it treats all particles as either deeply trapped or circulating with constant velocity.

In the next section we will show that the circulating particles contribution is much larger than that of the trapped particles when $\omega > \omega_{\text{T}}$. The opposite is true when $\omega < \omega_{\text{Bi}}$. Treating the particles in action angle space with the real motion removes the problem of the deeply trapped/well circulating particle approximation adopted here. It should also be noted that effects of trapped and circulating particles are not merely additive, since both types appear in $\delta\Phi_s$, which enters in both Λ_{cir}^2 and Λ_{tra}^2 . This confirms the fact that the dynamics response of the two types of particles is deeply connected.

The effects of the $\omega = \bar{\omega}_{\text{di}} \pm \omega_{\text{bi}}$ resonances in the kinetic layer are included in the $Z(\Omega_{1,2})$ functions; meanwhile, the $\omega = \bar{\omega}_{\text{di}}$ and $\omega = \bar{\omega}_{\text{de}}$ resonances, except for the I_{Φ} term as mentioned above, appear only in the ideal region and are mostly driven by the normal curvature, unlike the former.

5. Limiting cases and connection with GAM

For very low frequencies $|\omega| \ll \omega_{\text{Bi}}$ it is easy to show that

$$\delta\Phi_s \sim \sqrt{2\epsilon} \frac{\omega \bar{\omega}_{\text{Di}}}{\omega_{\text{Bi}}^2} \xi \delta\Phi^{(0)} \ll \xi \delta\Phi^{(0)}.$$

This means that $S(\omega, \bar{\omega}_{\text{Di}}, \omega_{\text{Bi}}, \omega_{\text{T}}) \rightarrow 0$ and thus the main contribution in Λ_{tra}^2 comes from the P_3 function in equation (24). The low-frequency limit of equation (24)

$$\Lambda^2/I_{\Phi} \simeq \frac{\omega^2}{\omega_{\text{A}}^2} \left(1 - \frac{\omega_{*pi}}{\omega} \right) \left(1 + \frac{15}{16} \sqrt{2} q^2 \epsilon^{-1/2} + 0.5 q^2 \right) \quad (25)$$

is then easily obtained by setting $\omega \rightarrow 0$ in Λ_{cir}^2 [7] and Λ_{tra}^2 . The $(15/16)\sqrt{2}q^2\epsilon^{-1/2}$ comes from the trapped particles response, accounting for $(3/4)\sqrt{2}q^2\epsilon^{-1/2}$, and from the circulating particle response near the trapped to passing boundary, accounting for $(3/16)\sqrt{2}q^2\epsilon^{-1/2}$. In this sense, we could interpret this last contribution as that of barely circulating particles, although all circulating particles are assumed to have $v_{\parallel} = \text{const}$ in our model. Meanwhile, $0.5q^2$ is the circulating particles response and $I_{\Phi} \simeq 1$. Remembering that $\epsilon^{-1/2} \gg 1$, this result confirms that the trapped particles contribution is dominant in this region, thus justifying the necessity of retaining their effect in the analysis.

The result of equation (25) can be compared with the low-frequency MHD result by Graves and Hastie [83]:

$$\Lambda^2 = \frac{\omega^2}{\omega_{\text{A}}^2} \left(1 - \frac{\omega_{*pi}}{\omega} \right) (1 + 1.6 q^2 \epsilon^{-1/2} + 0.5 q^2). \quad (26)$$

The difference between the factors 1.6 and $(15/16)\sqrt{2} \approx 1.3$ in the two equations is due to the treatment of all particles as deeply trapped/well circulating. Note also that, of the factor 1.6,

$\simeq 1.2$ is due to trapped while $\simeq 0.4$ is due to barely circulating particles [10]; thus, the present estimate based on deeply trapped/well circulating particles compares well with the expected results based on exact trapped particle orbits (see appendix A). Taking into account the exact bounce/transit motion of the particles produces elliptic integrals in the velocity space and gives the same result as [83] (see appendix A).

The high-frequency (fluid) limit can be obtained by setting $|\omega| \gg \omega_{Ti}$ in both Λ_{cir}^2 and Λ_{tra}^2 . If we consider only circulating particles, then the kinetic (inertial) layer response can be written as [7]

$$\Lambda_{\text{cir}}^2 = -\frac{\omega^2}{\omega_A^2} q^2 \frac{\omega_{Ti}^2}{\omega^2} \left[\left(\frac{7}{4} + \tau \right) - \frac{3}{4} \sqrt{2\epsilon} \left(\frac{5}{4} + \tau \right) \right] \quad (27)$$

for $\omega_{*pi}/\omega \rightarrow 0$. Note that the $\propto \sqrt{2\epsilon}$ terms describe the modified circulating particle response only, since the $S(\omega, \bar{\omega}_{Di}, \omega_{Bi}, \omega_{Ti})$ function becomes independent of $\sqrt{2\epsilon}$ at high frequency, as it is easily verified from equation (16). Following the same procedure and expanding the final result in $\omega_{Bi}/\omega \rightarrow 0$ we get

$$\Lambda_{\text{tra}}^2 = -\frac{3}{4} \sqrt{2\epsilon} \frac{\omega^2}{\omega_A^2} q^2 \frac{\omega_{Ti}^2}{\omega^2} \left(\frac{5}{4} + \tau \right), \quad (28)$$

the final line being obtained by setting $\omega_{*pi}/\omega \rightarrow 0$ and $\omega_B^2 = \epsilon \omega_T^2/2$ for thermal ion frequencies. As expected, we find that the trapped particles effect is of order $\sqrt{2\epsilon}$ with respect to that of the circulating particles and cancels the $\propto \sqrt{2\epsilon}$ terms in the circulating particle response at high frequency (see appendix B). Combining the two results, this gives [7]

$$\Lambda^2 = \frac{\omega^2}{\omega_A^2} \left[1 - q^2 \frac{\omega_{Ti}^2}{\omega^2} \left(\frac{7}{4} + \tau \right) \right]. \quad (29)$$

This result on the shear Alfvén continuous spectrum accumulation point ($\Lambda = 0$) at high frequency shows that trapped particles do not appreciably alter the dynamics for $|\omega| \gg |\omega_{Ti}|$. In fact, they introduce an $O(\epsilon)$ frequency shift, whereas they provide the dominant contribution to the plasma inertia at low frequency for $|\omega| \ll |\omega_{Bi}|$ [83]. These considerations are readily extended to GAM, by invoking the degeneracy of BAE and GAM spectra in the long wavelength limit ($\Lambda = 0$ and $\omega_{*pi} = 0$) [8–10, 42]. Based on our present findings, we may conclude that the GAM frequency shift due to trapped particles is $O(\epsilon)$.

6. Numerical studies of analytic expressions

The limiting expressions derived above and in appendix A, namely equations (25)–(29), are valid in the asymptotic sense; thus, it is important to quantitatively determine how reliable they are. Furthermore, it is difficult to visualize the effect of trapped particle dynamics on the low-frequency SAW continuous spectrum, due to the complicated form of equation (24). For these reasons, in this section we briefly present some numerical studies of analytic expressions based on equation (24), with the aim of discussing the effect of trapped particles on the structure of the continuous spectrum and on gap modes frequencies.

In general, being the form of the SAW continuous spectrum expressed in terms of transcendental functions, we can expect that there exists an infinite number of roots for the accumulation points ($\Lambda^2 = 0$). This is the case even for the simpler Λ^2 expression derived earlier, assuming only well circulating thermal ions [7]. From the physical point of view, this multitude of accumulation points is not an issue: what one can certainly state is that only accumulation points which are closest to the real axis (least damped) should be relevant. For

example, the BAAE accumulation point at $k_{\parallel}qR_0 = 0$, obtained in [69, 81] with the expression Λ^2 used in [7], is significantly more damped than the BAE accumulation point. What eventually determines which branch of the low-frequency SAW-SMW spectrum is preferentially excited is equation (1).

Since this section is not meant to be comprehensive, for it rather tries to isolate some important qualitative features due to trapped particles, we focus mainly on the low-frequency SAW continuous spectrum and Alfvén eigenmodes connected with the BAE accumulation point. In fact, this is the typical case of interest in present-day experiments looking at long wavelength and low to moderate mode numbers driven by energetic particle populations. Since the corresponding relevant frequencies are much larger than the thermal particle toroidal precession frequencies, we may consider $I_{\Phi} \simeq 1$ in equation (24). More comprehensive and exhaustive numerical studies of equation (1) using Λ^2 given by equation (24) will be reported elsewhere, discussing both lower frequency and shorter wavelength modes.

In figure 1, we show the real frequency dependence ($\Im\omega = 0$) of Λ^2 , given by equation (24), for two different values of ϵ , $\epsilon = 0$ (no trapped particles) and $\epsilon = 0.1$. Fixed parameters are $\omega_{*ni}/\omega_{Ti} = \omega_{*Ti}/\omega_{Ti} = 0.2$, $\tilde{\omega}_{Di}/\omega_{Ti} = 0.15/\sqrt{2}$, $q = 1.5$ and $\tau = 1$. As expected from equation (24), the precession-bounce resonance with trapped thermal ions affects the response at low frequencies. However, while the resonant wave-particle interaction becomes exponentially small at $|\omega| \gg \omega_{Ti}$ and $\Im\Lambda^2$ is not significantly modified by trapped particles at high frequencies, the non-resonant response $\Re\Lambda^2$ shows slower (algebraic) convergence to the asymptotic limit of equation (29). It has already been emphasized [65] that the validity range of the high-frequency limit of equation (29) is fairly limited. Here, we see that the residual $\propto \sqrt{\epsilon}$ difference between $\Re\Lambda^2$ expressions with and without trapped particles at high frequencies is due to the fact that equation (27) and (28) have different expansion parameters; so, exact cancellation of $\propto \sqrt{\epsilon}$ terms requires that the most stringent asymptotic expansion applies.

Results in figure 1 are useful to interpret the effect of trapped particle dynamics on the low-frequency SAW continuous spectrum and BAE modes. For the same fixed parameters of figure 1 and for fixed $v_{Ti}^2/v_A^2 = 0.01$, we have solved equation (1) for $\delta\hat{W}_f = -0.1$ and $\delta\hat{W}_f = -0.2$, obtaining the Alfvén eigenmode (BAE) frequency dependence on $\epsilon \in [0, 0.1]$. We also solved $\Lambda^2 = k_{\parallel}^2 q^2 R_0^2$, i.e. the SAW continuum structure, for $|k_{\parallel}qR_0| = 0.1$ and $|k_{\parallel}qR_0| = 0.2$. Results are reported in figures 2 and 3, where the dependences of $\Re(\omega/\omega_{Ti})$ and $\Im(\omega/\omega_{Ti})$ are shown versus ϵ , respectively, for both BAE (full circles and squares) and SAW continuous spectrum (empty circles and squares). For reference, the SAW continuum accumulation point ($\Lambda^2 = 0$; dashed line) is also shown. The BAE real frequency drop for increasing trapped particle population (ϵ), shown in figure 2, is qualitatively consistent with the recent numerical results obtained by means of the LIGKA code and used for analyzing BAE excited by ICRH energetic ions tails in AUG [29, 30]. This drop is explained as a consequence of the $\Re\Lambda^2$ behavior with and without trapped particles at high frequencies, displayed in figure 1. A similar explanation accounts for the behavior of SAW continuous spectrum frequency at finite $|k_{\parallel}qR_0|$ and at $|k_{\parallel}qR_0| = 0$. Meanwhile, the damping increase for increasing ϵ , visible in figure 3, is a consequence of the real frequency drop and the corresponding strengthening of wave-particle resonant interactions, although—for fixed (high) frequency—inclusion of trapped particles weakens the resonant wave-particle response, as shown in figure 1.

It is worth noting that figure 3 does not imply a stabilizing role of trapped particles; it suggests only that resonant wave-particle interactions are strengthened when trapped particle dynamics is included. This means that, above the excitation threshold of the Alfvénic ITG driven branch [7, 49, 50], modes could be more unstable with the inclusion of trapped particle

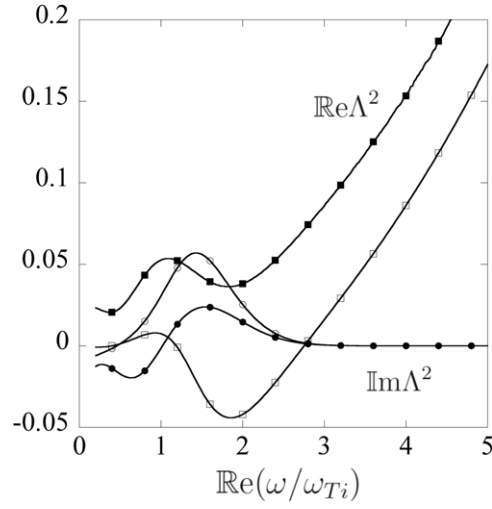


Figure 1. Values of $\Re\Lambda^2$ ($\epsilon = 0$ open squares; $\epsilon = 0.1$ full squares) and $\Im\Lambda^2$ ($\epsilon = 0$ open circles; $\epsilon = 0.1$ full circles) are shown versus $\Re(\omega/\omega_{Ti})$ for fixed parameters $\omega_{*ni}/\omega_{Ti} = \omega_{*ni}/\omega_{Ti} = 0.2$, $\bar{\omega}_{Di}/\omega_{Ti} = 0.15/\sqrt{2}$, $q = 1.5$ and $\tau = 1$.

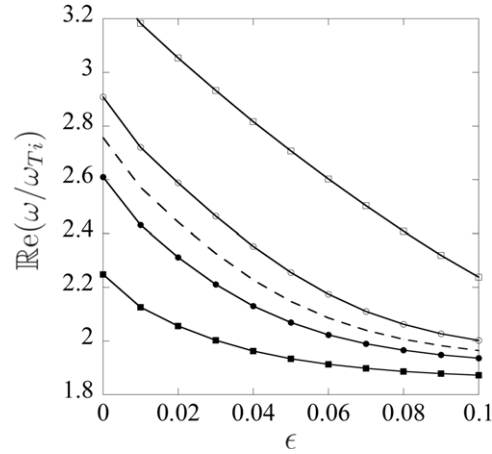


Figure 2. Dependence of SAW continuous spectrum and BAE real frequency on ϵ . Full symbols indicate BAE modes (full circles $\delta\tilde{W}_f = -0.1$; full squares $\delta\tilde{W}_f = -0.2$); empty symbols indicate the SAW continuous spectrum (empty circles $|k_{||}qR_0| = 0.1$; empty squares $|k_{||}qR_0| = 0.2$). The SAW continuum accumulation point at $|k_{||}qR_0| = 0$ is also shown as reference (dashed line). Fixed parameters are those of figure 1 and $v_{Ti}^2/v_A^2 = 0.01$.

response. These aspects are expected to be relevant for the analysis of drift Alfvén ballooning mode stability.

7. Conclusions and discussion

In section 4, we derived the kinetic layer wave equation and the corresponding expression of Λ , entering the general ‘fishbone-like’ dispersion relation equation (1), treating resonant wave-particle interactions and SAWs–SMWs on the same footing and extending the validity regime

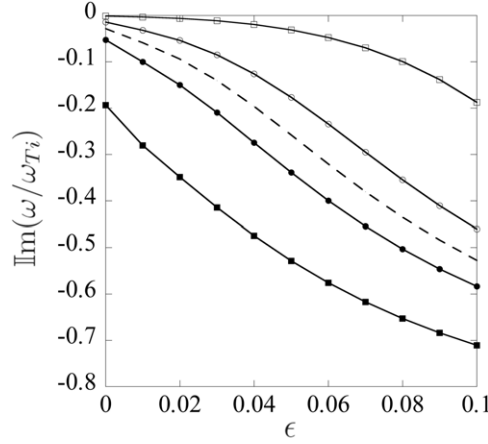


Figure 3. Dependence of SAW continuous spectrum and BAE damping rate (imaginary frequency) on ϵ . Full symbols indicate BAE modes (full circles $\delta\tilde{W}_f = -0.1$; full squares $\delta\tilde{W}_f = -0.2$); empty symbols indicate the SAW continuous spectrum (empty circles $|k_{||}qR_0| = 0.1$; empty squares $|k_{||}qR_0| = 0.2$). The SAW continuum accumulation point at $|k_{||}qR_0| = 0$ is also shown as reference (dashed line). Fixed parameters are those of figure 1 and $v_{Ti}^2/v_A^2 = 0.01$.

of prior analyses to the whole frequency range $0 < |\omega| \ll \omega_A$, i.e. including wave–particle interactions for both circulating and trapped thermal ions and for trapped thermal electrons.

In order to make the problem analytically tractable, we have assumed all trapped particles as deeply trapped and all circulating particles as well circulating. Despite this assumption, the theoretical description presented here captures the essential qualitative features of the structures of the low-frequency shear Alfvén continuous spectrum due to resonant wave–particle interactions with magnetically trapped thermal particles. The functional forms of asymptotic limits are reproduced at both low and high frequencies (see section 5 and appendix A), while relevant wave–particle interactions are maintained, allowing us to elucidate the important physics effects of trapped particles on the low-frequency structures of SAW continuous spectrum in toroidal geometry. In particular, we show that trapped particle contribution is not only important but becomes dominant at frequencies of the order of the thermal ion bounce frequency ω_{Bi} . This result was expected on the basis of the low-frequency expression of the MHD inertia enhancement [83]; however, in the light of our analysis and of other recent results on kinetic internal kink stability in ITER [82], it is evident that kinetic treatments of the thermal plasma components are needed for a realistic description of thermonuclear plasmas, where SAWs, MHD and DWT will characterize complex behavior mediated by their mutual interactions.

One important conclusion, which may be drawn on the basis of the present theoretical analysis, is that the kinetic layer thermal ion dynamic response in the kinetic thermal ion (KTI) gap frequency range is dominated by geodesic curvature, i.e. by transit and/or precession-bounce resonances. Thermal particle precession resonance enters mainly via the non-vanishing ‘flute-like’ component ($|k_{||}qR_0| \ll 1$) of the parallel electric field, which is negligibly small at $|\omega| \gg |\tilde{\omega}_{Di}|, |\tilde{\omega}_{De}|$.

The general expression for Λ , equation (24) obtained in this work, can be readily used in connection with equation (1) for analyzing a number of kinetic stability problems involving SAWs, MHD and Alfvénic DWT. In fact, since there is a continuous transition between various SAW and MHD fluctuation branches in many situations of experimental interest, the results

reported in this work are of practical relevance for their interpretation. Such detailed analyses are, however, beyond the scope of this work and will be a subject of future investigations.

Acknowledgments

Useful discussions with A Biancalani and C Di Troia are kindly acknowledged. This work was supported by the Euratom Communities under the contract of Association between EURATOM/ENEA. This work was partly carried out within the framework of the SciDAC Gyrokinetic Simulation of Energetic Particle Turbulence and Transport (GSEP) project and partly supported by the ‘Consorzio di Ricerca per l’Energia e le Applicazioni Tecnologiche dell’Elettromagnetismo’ (CREATE). One of the authors (IC) would like to thank the Italian Ministry of Foreign Affairs for financing his graduate studies, during which this research was conducted.

Appendix A. General derivation of limiting cases

Here, we briefly sketch the general derivation of limiting cases of the Λ expression discussed in section 5. In fact, both low- [83] and high-frequency [7] limits are analyzed in the literature; so, we briefly report these known results for the readers’ convenience and for comparison with the approximate expressions derived in section 5. Discrepancies between general limiting forms and approximate asymptotic expressions are due to the fact that, in this work, we have treated all trapped particles as deeply trapped and all circulating particles as well circulating. Despite this assumption, as specified in section 1, the theoretical description presented here captures the essential qualitative features of the relevant wave–particle interactions and correctly reproduces functional forms of asymptotic limits at both low [83] and high [7] frequencies, allowing us to elucidate the important physics effects of trapped particles on the low-frequency structures of SAW continuous spectrum in toroidal geometry, while keeping technical difficulties to a minimum.

To analyze the different roles of trapped and circulating particles, we move from (ε, χ) to (ε, κ^2) space, with $\chi = \mu B_0/\varepsilon$ and

$$\kappa^2 = \frac{2(r/R_0)\chi}{1 - (1 - r/R_0)\chi}, \quad (\text{A.1})$$

$\kappa^2 < 1$ [$0 \leq \chi < (1 - r/R_0)$] indicating circulating particles, while trapped particles have $\kappa^2 > 1$ [$(1 - r/R_0) < \chi \leq (1 + r/R_0)$]. With these new velocity space variables, it is easily shown that

$$\begin{aligned} \int d\mathbf{v}(\dots) = \langle(\dots)\rangle &= 2\pi(r/R_0)^{1/2} \sum_{v_{\parallel}/|v_{\parallel}|=\pm} \int_0^{\infty} \varepsilon^{1/2} d\varepsilon \\ &\times \int_0^{\infty} d\kappa^2 (1 - \kappa^2 \sin^2(\theta/2))^{-1/2} \frac{(\dots)}{[\kappa^2 + 2r/R_0]^{3/2}}. \end{aligned} \quad (\text{A.2})$$

For integrands (\dots) independent of κ^2 (and similarly for given κ^2 dependences), it is possible to transform equation (A.2) into a simplified asymptotic form by further separating well circulating particles with $\kappa^2 \lesssim \delta = O[(r/R_0)^{1/2}]$ from others:

$$\begin{aligned} \int d\mathbf{v}(\dots) = \langle(\dots)\rangle &= 2\pi \sum_{v_{\parallel}/|v_{\parallel}|=\pm} \int_0^{\infty} (2\varepsilon)^{1/2} d\varepsilon \left\{ 1 + (2r/R_0)^{1/2} \right. \\ &\times \left. \left[-\frac{1}{\delta^{1/2}} + \int_{\delta}^{\infty} \frac{d\kappa^2}{2\kappa^3} (1 - \kappa^2 \sin^2(\theta/2))^{-1/2} \right] \right\} (\dots). \end{aligned} \quad (\text{A.3})$$

This last equation, when used as identity, demonstrates that the quantity in square parentheses must vanish for normalization constraints.

From [7, 10], it is easily shown that the general expression of Λ is related to the inertia enhancement and can be written in compact form as

$$\frac{\omega^2}{\omega_A^2} \left(1 - \frac{\omega_{*pi}}{\omega}\right) \partial_r^2 \delta\phi \rightarrow \left[\frac{\omega^2}{\omega_A^2} \left(1 - \frac{\omega_{*pi}}{\omega}\right) + \Delta I \right] \partial_r^2 \delta\phi, \quad (\text{A.4})$$

where

$$\Delta I \partial_r^2 \delta\phi = \oint \frac{d\theta}{2\pi} \left\langle \frac{4\pi}{c^2} e q^2 R_0^2 \omega \omega_{di} \delta K_i \right\rangle. \quad (\text{A.5})$$

In the low-frequency limit, $|\omega| \ll \omega_{Bi} \approx (r/R_0)^{1/2} \omega_{Ti}$, following [83] one readily obtains

$$\Delta I = q^2 \frac{\omega^2}{\omega_A^2} \left(1 - \frac{\omega_{*pi}}{\omega}\right) \left(\frac{R_0}{r}\right)^{1/2} f\left(\frac{r}{R_0}\right), \quad (\text{A.6})$$

where, at the lowest order in (r/R_0) [10],

$$\begin{aligned} f\left(\frac{r}{R_0}\right) &\simeq 1.6 \simeq \frac{6\sqrt{2}}{\pi} \int_{\delta}^1 \frac{d\kappa^2}{\kappa^5} \left[\mathbb{E}(\kappa) - \frac{\pi^2}{4\mathbb{K}(\kappa)} \right] + \frac{3}{8\sqrt{2}} \delta^{1/2} \\ &+ \frac{6\sqrt{2}}{\pi} \int_1^{\infty} \frac{d\kappa^2}{\kappa^6} \left[(1 - \kappa^2) \mathbb{K}(1/\kappa) + \kappa^2 \mathbb{E}(1/\kappa) \right]. \end{aligned} \quad (\text{A.7})$$

Here, $\mathbb{K}(\kappa)$ and $\mathbb{E}(\kappa)$ are the complete elliptic integrals of the first and second kinds, respectively. Since $\delta = O[(r/R_0)^{1/2}]$, the first two terms on the rhs represent the contribution of barely circulating particles ($\simeq 0.43$), while the last term on the rhs ($\simeq 1.20$) comes from trapped particles [10]. Note that the structure of equation (A.7) is the same as that involved in the ZF polarizability [89, 90], as expected. The discrepancy between the exact lowest order value $f(r/R_0) = 1.6$ and the approximate value $f(r/R_0) = (15/16)\sqrt{2}$, given by equation (25), is to be attributed to the deeply trapped/well circulating particle simplified description. Actually, the value $(3/4)\sqrt{2} \approx 1.1$, coming from deeply trapped particles, should be compared with the precise trapped particle contribution $\simeq 1.2$, while the value $(3/16)\sqrt{2} \approx 0.27$, coming from circulating particle near the trapped to passing boundary, should correspond to the barely circulating particle response $\simeq 0.43$. Here, as an independent check of the results reported in this work, we also note that the values predicted for trapped $((3/4)\sqrt{2})$ and barely passing $((3/16)\sqrt{2})$ particles can be directly obtained from the exact expression reported in equation (A.7), assuming small argument expansion for elliptic integrals, which corresponds to the deeply trapped/well circulating particle simplified description, adopted here. At next order $f(r/R_0) = 1.6 + 0.5(r/R_0)^{1/2}$, so that equation (A.4) coincides with equation (26) [83].

In the high-frequency limit, $\omega_{Ti} \ll |\omega| \ll \omega_A$, we follow [7] and readily obtain

$$\delta K_i = 2 \frac{\sin \theta}{k_{\theta}} (i \partial_r \delta\phi) \frac{\omega_{Di}}{\omega} \left[\tau + \frac{m_i}{2T_i} \left(\frac{v_{\perp}^2}{2} + v_{\parallel}^2 \right) \right] \frac{e}{T_i} f_{0i}. \quad (\text{A.8})$$

Here, we have considered that $\omega_{di} = (m_i/T_i) \omega_{Di} (v_{\perp}^2/2 + v_{\parallel}^2) (nq)^{-1} i \sin \theta (r \partial_r)$ in the kinetic layer region. In this way, straightforward application of equation (A.5) gives

$$\Delta I \partial_r^2 \delta\phi = - \left(\frac{7}{4} + \tau \right) q^2 \frac{\omega_{Ti}^2}{\omega_A^2} \partial_r^2 \delta\phi, \quad (\text{A.9})$$

which yields the Λ^2 expression of equation (27). Thus, the simplified model description of particle orbits, adopted here, precisely reproduces the high-frequency limit.

Appendix B. Modified circulating ion response due to finite trapped particle fraction

Strictly following [7], the functions $D_1(x)$, $N_1(x)$, $F(x)$ and $G(x)$, defined here in equations (17), (18) and (21), are given by the following expressions:

$$\begin{aligned}
 D_1(x) &= \frac{x}{\sqrt{\pi}} \int_0^\infty dy \int_{-\infty}^\infty dz e^{-y-z^2} \left[\left(1 - \frac{\omega_{*ni}}{x\omega_{Ti}} \right) - \frac{\omega_{*Ti}}{x\omega_{Ti}} \left(y + z^2 - \frac{3}{2} \right) \right] \frac{1}{z-x}, \\
 N_1(x) &= \frac{\bar{\omega}_{Di}/\omega_{Ti}}{\sqrt{\pi}} \int_0^\infty dy \int_{-\infty}^\infty dz e^{-y-z^2} \left[\left(1 - \frac{\omega_{*ni}}{x\omega_{Ti}} \right) - \frac{\omega_{*Ti}}{x\omega_{Ti}} \left(y + z^2 - \frac{3}{2} \right) \right] \frac{y+2z^2}{z-x}, \\
 F(x) &= \frac{1}{\sqrt{\pi}} \int_0^\infty dy \int_{-\infty}^\infty dz e^{-y-z^2} \frac{(y/2+z^2)^2}{z-x}, \\
 G(x) &= \frac{1}{\sqrt{\pi}} \int_0^\infty dy \int_{-\infty}^\infty dz e^{-y-z^2} \left(y + z^2 - \frac{3}{2} \right) \frac{(y/2+z^2)^2}{z-x}. \tag{B.1}
 \end{aligned}$$

In order to evaluate the modified circulating ion response due to finite trapped particle fraction, the above integral must be computed excluding the trapped particle cone $-\sqrt{2\epsilon y} \leq z \leq \sqrt{2\epsilon y}$. Moreover, since our approach is valid up to $O(\epsilon^{1/2})$ with respect to the leading term, $z^2 = O(\epsilon)$ terms can be dropped inside the trapped particle cone, leaving a trivial integration in z to perform and yielding the modified circulating ion response expressed as $D_1(x) \rightarrow D_1(x) + \Delta D_1(x)$, $N_1(x) \rightarrow N_1(x) + \Delta N_1(x)$, $F(x) \rightarrow F(x) + \Delta F(x)$ and $G(x) \rightarrow G(x) + \Delta G(x)$, with

$$\begin{aligned}
 \Delta D_1(x) &= \frac{x}{\sqrt{\pi}} \int_0^\infty e^{-y} \ln \left(\frac{x + \sqrt{2\epsilon y}}{x - \sqrt{2\epsilon y}} \right) \left[\left(1 - \frac{\omega_{*ni}}{x\omega_{Ti}} \right) - \frac{\omega_{*Ti}}{x\omega_{Ti}} \left(y - \frac{3}{2} \right) \right] dy, \\
 \Delta N_1(x) &= \frac{\bar{\omega}_{Di}/\omega_{Ti}}{\sqrt{\pi}} \int_0^\infty y e^{-y} \ln \left(\frac{x + \sqrt{2\epsilon y}}{x - \sqrt{2\epsilon y}} \right) \left[\left(1 - \frac{\omega_{*ni}}{x\omega_{Ti}} \right) - \frac{\omega_{*Ti}}{x\omega_{Ti}} \left(y - \frac{3}{2} \right) \right] dy, \\
 \Delta F(x) &= \frac{1}{\sqrt{\pi}} \int_0^\infty \frac{y^2}{4} e^{-y} \ln \left(\frac{x + \sqrt{2\epsilon y}}{x - \sqrt{2\epsilon y}} \right) dy, \\
 \Delta G(x) &= \frac{1}{\sqrt{\pi}} \int_0^\infty \frac{y^2}{4} \left(y - \frac{3}{2} \right) e^{-y} \ln \left(\frac{x + \sqrt{2\epsilon y}}{x - \sqrt{2\epsilon y}} \right) dy. \tag{B.2}
 \end{aligned}$$

which coincide with the definitions given in equations (19), (20), (22) and (23).

References

- [1] Heidbrink W W, Strait E J, Chu M S and Turnbull A D 1993 *Phys. Rev. Lett.* **71** 855
- [2] Turnbull A D *et al* 1993 *Phys. Fluids B* **5** 2546
- [3] Heidbrink W W 2002 *Phys. Plasmas* **9** 2113
- [4] Chen L, White R B and Rosenbluth M N 1984 *Phys. Rev. Lett.* **52** 1122
- [5] Tsai S T and Chen L 1993 *Phys. Fluids B* **5** 3284
- [6] Chen L 1994 *Phys. Plasmas* **1** 1519
- [7] Zonca F, Chen L and Santoro R A 1996 *Plasma Phys. Control. Fusion* **38** 2011
- [8] Zonca F and Chen L 2006 *Plasma Phys. Control. Fusion* **48** 537
- [9] Chen L and Zonca F 2007 *Nucl. Fusion* **47** S727
- [10] Zonca F *et al* 2007 *Nucl. Fusion* **47** 1588
- [11] Chen L 2008 *Plasma Phys. Control. Fusion* **50** 124001
- [12] Nguyen C, Garbet X and Smolyakov A I 2008 *Phys. Plasmas* **15** 112502
- [13] Heidbrink W W 2008 *Phys. Plasmas* **15** 055501
- [14] Sharapov S E *et al* 2001 *Phys. Lett. A* **289** 127
- [15] Berk H L *et al* 2001 *Phys. Rev. Lett.* **87** 185002

- [16] Takechi M *et al* 2002 Property of Alfvén eigenmode in JT-60U reversed shear and weak shear discharges *Proc. 19th Int. Conf. on Fusion Energy 2002 (Lyon, France, 2002)* (Vienna: IAEA) CD-ROM file EX/W-6 and <http://www.iaea.org/programmes/ripc/physics/fec2002/html/fec2002.htm>
- [17] Nazikian R *et al* 2006 *Phys. Rev. Lett.* **96** 105006
- [18] Breizman B N *et al* 2005 *Phys. Plasmas* **12** 112506
- [19] Nabais F *et al* 2005 *Phys. Plasmas* **12** 102509
- [20] Zonca F, Chen L, Botrugno A, Buratti P, Cardinali A, Cesario R, Pericoli Ridolfini V and JET EFDA Contributors 2009 *Nucl. Fusion* **49** 085009
- [21] Buratti P *et al* 2005 *Nucl. Fusion* **45** 1446
- [22] Annibaldi S V, Zonca F and Buratti P 2007 *Plasma Phys. Control. Fusion* **49** 475
- [23] Zimmermann O *et al* 2005 *Proc. 32nd EPS Conf. on Plasma Physics and Controlled Fusion (Tarragona, Spain)* P4-059
- [24] Gorelenkov N N, Berk H L, Fredrickson E and Sharapov S E 2007 *Phys. Lett. A* **370** 70
- [25] Gorelenkov N N *et al* 2007 *Plasma Phys. Control. Fusion* **49** B371
- [26] Garcia-Munoz M *et al* 2008 *Phys. Rev. Lett.* **100** 055005
- [27] Garcia-Munoz M *et al* 2008 MHD induced Fast-Ion Losses on ASDEX Upgrade *Proc. 22nd Int. Fusion Energy Conf. 2008 (Geneva, Switzerland, 2008)* (Vienna: IAEA) CD-ROM file EX/6-1
- [28] Lauber Ph *et al* 2008 *35th EPS Conf. on Plasma Phys. (Hersonissos, Crete, Greece, 9–13 June 2008)* vol 32 (ECA) O-4.030
- [29] Lauber Ph *et al* 2009 Kinetic Alfvén eigenmodes at ASDEX Upgrade *Plasma Phys. Control. Fusion* submitted
- [30] Lauber Ph *et al* 2009 Damping and drive of Alfvén eigenmodes at ASDEX Upgrade *36th EPS Conf. on Plasma Phys. (Sofia, Bulgaria, 29 June–3 July 2009)* I-5.077
- [31] Sabot R *et al* 2008 Observation of fast particles modes in Tore-Supra *Proc. 22nd Int. Fusion Energy Conf. 2008 (Geneva, Switzerland 2008)* (Vienna: IAEA) CD-ROM file EX/P8-9
- [32] Jakubowski M *et al* 2002 *Phys. Rev. Lett.* **89** 265003
- [33] Schoch P M *et al* 2003 *Rev. Sci. Instrum.* **74** 1846
- [34] Fujisawa A *et al* 2004 *Phys. Rev. Lett.* **93** 165002
- [35] Hamada Y *et al* 2005 *Nucl. Fusion* **45** 81
- [36] Melnikov A V *et al* 2006 *Plasma Phys. Control. Fusion* **48** S87
- [37] Ido T *et al* 2006 *Nucl. Fusion* **46** 512
- [38] Conway G D *et al* 2005 *Plasma Phys. Control. Fusion* **47** 1165
- [39] Zhao J *et al* 2006 *Phys. Rev. Lett.* **96** 255004
- [40] Krämer-Flecken A, Soldatov S, Reiser D, Kantor M and Koslowski H R 2009 *Plasma Phys. Control. Fusion* **51** 015001
- [41] Zonca F *et al* 2006 *Plasma Phys. Control. Fusion* **48** B15
- [42] Zonca F 2008 *Int. J. Mod. Phys. A* **23** 1165
- [43] Zonca F and Chen L 2008 Structures of the low frequency Alfvén continuous spectrum and their consequences on MHD and micro-turbulence Theory of Fusion Plasmas *AIP Conf. Proc.* **1069** 355
- [44] Zonca F and Chen L 2008 Nonlinear Dynamics and Complex Behaviors in Magnetized Plasmas of Fusion Interest *Frontiers in Modern Plasma Physics AIP Conf. Proc.* **1061** 34
- [45] Hasegawa A, MacLennan C G and Kodama Y 1979 *Phys. Fluids* **22** 2122
- [46] Winsor N, Johnson J L and Dawson J M 1968 *Phys. Fluids* **11** 2448
- [47] Zonca F, Briguglio S, Chen L, Fogaccia G and Vlad G 2000 *Theory of Fusion Plasmas* ed J W Connor *et al* (Bologna: SIF) p 17
- [48] Zonca F, Briguglio S, Chen L, Fogaccia G and Vlad G 2005 *Nucl. Fusion* **45** 477
- [49] Zonca F, Chen L, Santoro R A and Dong J Q 1998 *Plasma Phys. Control. Fusion* **40** 2009
- [50] Zonca F, Chen L, Dong J Q and Santoro R A 1999 *Phys. Plasmas* **6** 1917
- [51] Fredrickson E D *et al* 2006 *Phys. Plasmas* **13** 056109
- [52] Günter S *et al* 2007 *Nucl. Fusion* **47** 920
- [53] Heidbrink W W *et al* 2007 *Phys. Rev. Lett.* **99** 245002
- [54] Heidbrink W W *et al* 2008 *Nucl. Fusion* **48** 084001
- [55] Darrow D S *et al* 2008 *Nucl. Fusion* **48** 084004
- [56] Van Zeeland M A *et al* 2008 Alfvénic instabilities and fast ion transport in the DIII-D tokamak *Proc. 22nd Int. Fusion Energy Conf. 2008 (Geneva, Switzerland, 2008)* (Vienna: IAEA) CD-ROM file EX/6-2
- [57] Fredrickson E D *et al* 2008 Toroidal Alfvén Eigenmode Avalanches in NSTX *Proc. 22nd Int. Fusion Energy Conf. 2008 (Geneva, Switzerland, 2008)* (Vienna: IAEA) CD-ROM file EX/6-3
- [58] Berk H L *et al* 2006 *Nucl. Fusion* **46** S888
- [59] Garbet X *et al* 2006 Theory of Fusion Plasmas *AIP Conf. Proc.* **871** 342

- [60] Fu G Y 2007 *49th APS-DPP Annual Meeting (Orlando, FL)* B12.00004
- [61] Fu G Y 2008 *Phys. Rev. Lett.* **101** 185002
- [62] Fu G Y *et al* 2008 Energetic particle-induced geodesic acoustic mode *Proc. 22nd Int. Fusion Energy Conf. 2008 (Geneva, Switzerland, 2008)* (Vienna: IAEA) CD-ROM file TH/P3-15
- [63] Zonca F, Chen L and Qiu Z 2008 Kinetic theory of geodesic acoustic modes: radial structures and nonlinear excitations *Proc. 22nd Int. Fusion Energy Conf. 2008 (Geneva, Switzerland, 2008)* (Vienna: IAEA) CD-ROM file TH/P3-7
- [64] Smolyakov A I, Garbet X, Falchetto G and Ottaviani M 2008 *Phys. Lett. A* **372** 6750
- [65] Zonca F and Chen L 2008 *Europhys. Lett.* **83** 35001
- [66] Cheng C Z, Gorelenkov N N and Hsu C T 1995 *Nucl. Fusion* **35** 1639
- [67] Chen L and Zonca F 1995 *Phys. Scr. T* **60** 81
- [68] Zonca F and Chen L 1996 *Phys. Plasmas* **3** 323
- [69] Gorelenkov N N *et al* 2008 Theory and observations of low frequency eigenmodes due to Alfvén acoustic coupling in toroidal fusion plasmas *Proc. 22nd Int. Fusion Energy Conf. 2008 (Geneva, Switzerland, 2008)* (Vienna: IAEA) CD-ROM file TH/5-2
- [70] Cheng C Z, Chen L and Chance M S 1985 *Ann. Phys.* **161** 21
- [71] Chen L 1988 *Theory of Fusion Plasmas* (Bologna: SIF) 327
- [72] Boswell C J *et al* 2006 *Phys. Lett. A* **358** 154
- [73] Nazikian R *et al* 2008 *Phys. Rev. Lett.* **101** 185001
- [74] Smolyakov A I, Nguyen C and Garbet X 2008 *Plasma Phys. Control. Fusion* **50** 115008
- [75] Mikhailovskii A B and Sharapov S E 1999 *Plasma Phys. Rep.* **25** 838
- [76] Connor J W and Chen L 1985 *Phys. Fluids* **28** 2201
- [77] Sugama H and Watanabe T-H 2006 *Phys. Plasmas* **13** 012501
- [78] Gao Z, Itoh K, Sanuki H and Dong J Q 2006 *Phys. Plasmas* **13** 100702
- [79] Qiu Z Y, Chen L and Zonca F 2009 *Plasma Phys. Control. Fusion* **51** 012001
- [80] Gorelenkov N N 2008 *50th APS-DPP Annual Meeting (Dallas, TX)* G11.00002
- [81] Gorelenkov N N *et al* 2009 *Phys. Plasmas* **16** 056107
- [82] Hu B, Betti R and Manickam J 2006 *Phys. Plasmas* **13** 112505
- [83] Graves J P, Hastie R J and Hopcraft K I 2000 *Plasma Phys. Control. Fusion* **42** 1049
- [84] Glasser A H, Green J M and Johnson J L 1975 *Phys. Fluids* **18** 875
- [85] Mikhailovskii A B and Suramlishvili G I 1979 *Sov. J. Plasma Phys.* **5** 523
- [86] Mikhailovskii A B and Tsypin V S 1983 *Sov. J. Plasma Phys.* **9** 91
- [87] Belikov V S, Kolesnischenko Ya I and Silivra O A 1992 *Nucl. Fusion* **32** 1399
- [88] Bondeson A and Chu M S 1996 *Phys. Plasmas* **3** 3013
- [89] Rosenbluth M N and Hinton F L 1998 *Phys. Rev. Lett.* **80** 724
- [90] Hinton F L and Rosenbluth M N 1999 *Plasma Phys. Control. Fusion* **41** A653
- [91] Connor J W, Hastie R J and Taylor J B 1978 *Phys. Rev. Lett.* **40** 396
- [92] Antonsen T M and Lane B 1980 *Phys. Fluids* **23** 1205
- [93] Chen L and Hasegawa A 1991 *J. Geographical Res.* **96** 1503
- [94] Zonca F and Chen L 2000 *Phys. Plasmas* **7** 4600